Master's thesis

NTNU
Norwegian University of Science and Technology
Faculty of Natural Sciences
Department of Physics

Ola Nielsen Estensen

Controlling nuclear field gradients in triple quantum dot by Landau-Zener sweeps

Master's thesis in Ms.Phys.
Supervisor: Jeroen Danon
May 2019

NTNU
Kunnskap for en bedre verden

Ola Nielsen Estensen

Controlling nuclear field gradients in triple quantum dot by Landau-Zener sweeps

Master's thesis in Ms.Phys.
Supervisor: Jeroen Danon
May 2019

Norwegian University of Science and Technology
Faculty of Natural Sciences
Department of Physics

Abstract

Triple-spin quantum dots in GaAs have been proposed as a candidate quantum bit. The limitations of these systems are the coherence times of quantum states which are heavily affected by hyperfine interaction with nuclei in the GaAs host material. These nuclear fields oscillate in a random fashion causing dephasing of the quantum state and loss of information. In this thesis we explore the possibility of reducing these random oscillations through Landau-Zener sweeps between the logical state $|0\rangle$ and the $|Q_{3/2}\rangle$ state, causing spin-flips in the nuclear spin bath.

A Hubbard Hamiltonian is assumed which leads to the charge stability diagram of the system. This diagram shows the possible transitions between electron charge configuration across the three dots as a function of the applied voltages on each dot. Making using of these diagram we can determine where to tune the system to restrict the configurations to $(1,0,2)$, $(1,1,1)$ and $(2,0,1)$ which in turn gives the possible states of the system. These states can be sorted in different spin-subspaces, and we make the choice of using the $S_z = 1/2$ subspace with addition of $|Q_{3/2}\rangle$ which resides in the $S_z = 3/2$ sub-space. This will then amount to a total of six states in our basis.

The eigenstates of the system can be calculated numerically and the logical basis of our quantum bit $\{|0\rangle, |1\rangle\}$ will be the lowest lying states of the $S_z = 1/2$ subspace. Due to the different Zeeman-energies of $|0\rangle$ and $|Q_{3/2}\rangle$ these states can have an energy crossing depending on an external magnetic field applied over the system. Making use of this energy crossing Landau-Zener transitions between the corresponding states are possible, changing the electron spin in exchange for a spin-flip in one of the surrounding nuclei.

The effective magnetic field affects the crossing point of the two states, and will depend on the spin-flips. This crossing point again determines the probability of transition and a feedback mechanism is created. We make use of the numerical solution to $|0\rangle$ when calculating the transition probabilities and exploit smart sweep procedures to show that the nuclear field fluctuations can be suppressed in this way. This invites for a method of increasing the coherence

time of the system which ultimately determines the usability of the quantum bit.

We were also able to approximate the logical state $|0\rangle$ with an analytic expression through perturbation theory in the absence of nuclear field gradients. The resulting expression is valid for all ϵ, showing promise as a first step toward analytic understanding of the time dynamics of the polarisation due to the Landau-Zener sweeps.

Sammendrag

Trippel-spin kvanteprikker i GaAs har tidligere blitt foreslått som kandidat til kvante bit. Begrensningene til slike systemer følger av den hyperfine interaksjonen mellom elektronene og atomkjernene i vertsmaterialet, som forårsaker tap av fasen til elektronenes kvantetilstand og dermed tap av informasjon. Det effektive feltet atomkjernene utøver på elektronene vil svinge tilfeldig som gjør det vanskelige å kompensere for. I denne avhandlingen vil vi se på muligheten for å begrense størrelsen på disse svingningene gjennom Landau-Zener overganger mellom tilstanden $|0\rangle$ og $|Q_{3/2}\rangle$, som vil forårsake forandring av spin-retningen til atomkjernene.

En Hubbard Hamilton-funksjon vil bli brukt og leder til stabilitets-diagram for ladning over de tre prikkene. Dette diagrammet viser de mulige overgangene mellom elektron konfigurasjoner på prikkene som funksjon av det elektroniske potensialet man setter over hver av dem. Ved hjelp av dette diagrammet kan man begrense de mulige tilstandene til systemet ved å tilpasse potensialene. Vi vil bruke konfigurasjonene $(2,0,1)$,$(1,1,1)$ og $(1,0,2)$ som deretter angir de mulige tilstandene. Disse tilstandene kan deles inn i forskjellige grupper med forskjellige spin-tall S_z og vi vil bruke tilstandene som tilhører $S_z = 1/2$ og $S_z = 3/2$. Dette vil utgjøre totalt seks tilstander.

Egentilstandene til systemet kan bli funnet ved hjelp av numeriske metoder og vårt valg av logiske tilstander $\{|0\rangle, |1\rangle\}$ vil utgjøre de to laveste tilstandene med $S_z = 1/2$. På grunn av forskjellen i Zeeman-energi mellom $|0\rangle$ og $|Q_{3/2}\rangle$ kan man oppnå et krysningspunkt i energiene deres ved å justere et ytre magnetisk felt. Dette krysningspunktet kan brukes i Landau-Zener overganger for å endre orientering til elektronets spin, som igjen vil resultere i en endring i atomkjernenes spin.

The effektive magnetiske feltet som utøves på elektronene vil påvirke krysningspunktet til energiene. Dette feltet er igjen påvirket av spin-tilstanden til atomkjernene og dette fører sammen til en tilbakekoblingsprosess. For å simulere effecten av denne prosessen anvender vi den numerisk beregnede $|0\rangle$ og drar nytte av smarte metoder for å sveipe gjennom krysningspunktet. Dette vil

vi vise har en effekt på svingningene til det effektive feltet fra atomkjernenes spin som indikerer at en slik metode kan anvendes for å minske effekten av den hyperfine interaksjonen. Slik redusering er fundamentalt for å anvende slike systemer som kvante bit.

Vi presenterer også et analytisk uttrykk for $|0\rangle$ funnet gjennom perturbasjonsteori som gjelder for alle ϵ, hvis man antar fravær av hyperfin interaksjon. Dette er et første steg i analytisk forståelse av tids dynamikken til polariseringen som følge av Landau-Zener overganger.

Preface

This thesis culminates five years of study at the Norwegian University of Science and Technology. I would especially give thanks to my supervisor Jeroen Danon for his guidance and patience over the past year. Gratitude is also due for the invaluable discussions I have had with Vasil Saroka throughout the work with this thesis.

Trondheim, May 15, 2019
Ola Nielsen Estensen

Contents

Abbreviations

2DEG = Two-dimensional electron gas
AlGaAs = Aluminium Gallium Arsenide
CI = Constant-interaction model
GaAs = Gallium Arsenide
HEMT = High electron mobility transistor
HI = Hyperfine interaction
LZ = Landau-Zener
Qubit = Quantum bit
Si = Silicone
SOI = Spin-orbit interaction
TQD = Triple quantum dot
XOR = Exclusive OR

Chapter 1

Introduction

Towards the end of the 19th century classical physics was still believed sufficient to answer the mysteries of nature. In 1803 Thomas Young had shown the wavelike nature of light through interference in his double slit experiment, contradicting Isaac Newtons corpuscular (particle) theory. In 1873 James Clerk Maxwell published "A Treatise on Electricity and Magnetism" including the now famous Maxwell's equations. These equations would be proven experimentally by Heinrich Hertz in the 1880s. These things combined solidified the view of light as waves, and not particles.

The apparent strong foundation would however start to crack. Hydrogen gas would give off light with very specific wavelengths (spectrum lines) when heated. Heinrich Hertz had through his experiments [1] observed that metal would emit electrons when hit with light having sufficient frequency. Phillip Lenard would follow up on Hertz's work and discover that the kinetic energy of such emitted electrons would solely depend on the frequency, independent of the intensity. Another issue was the radiation from a black-body. The closest classical considerations had gotten was Wien's approximation which would shy away from experimental results for small frequencies. The solution to black-body radiation would mark the birth of quantum mechanics.

Of many scientists trying to figure out the discrepancy between theory and experiments, Max Planck introduced in 1900 a formula which was in accordance with the experimental results. The problem was however that he initially had no justification for it, it just seemed to fit. This formula is perhaps what Planck is most known for today, and called simply Planck's law

$$I(\nu, T) = \frac{2h\nu^3}{c^2} \frac{1}{e^{\frac{h\nu}{kT}} - 1} \tag{1.1}$$

It includes three constants of nature. Boltzmann's constant k, the velocity of light c (not known to be constant at the time) and Planck's constant h which

he introduced. The equation describes the intensity of light as a function of frequency ν and temperature T. Planck would continue work on the problem and by the end of 1900 he would present the results with a revolutionary assumption. The formula could be derived by assuming the radiation could only change its energy by incremental steps given by $E = h\nu$, where h is known as Planck's constant and ν is the frequency of light, and thus quantum mechanics had made its first steps despite Planck considering this a mere mathematical trick.

Albert Einstein would in the same period look into the discoveries of Hertz and Lenard regarding light and metallic surfaces, the photoelectric effect. Einstein proposed a solution[2] to the problem by postulating that electromagnetic radiation is dividable into a finite number of 'light quanta' (the term photon would in 1926 be coined by Gilbert Newton Lewis[3]). The light quanta would carry energy $E = h\nu$, in accordances to Planck's 'mathematical trick'. Further Einstein stated that each electron would be hit by only one such quanta of light such that the intensity of the light beam would make no difference for the individual electrons. It was for this work Einstein received his Nobel's price in physics in 1921.

The idea of quantisation also allowed Niels Bohr to develop his model for electrons orbiting a small dense nucleus. The structure of the atom was already known due to Ernest Rutherfords gold foil experiment in 1911, and a formula of the hydrogen emission lines had been formulated by Johannes Rydberg back in 1888. The Bohr model of the atom however introduced a theoretical explanation of these phenomenons. A key point was that electrons could only occupy specific orbits, and it was impossible for the electron to be inbetween two such orbits. Further would electrons in the innermost orbit remain stable there and emit no radiation.

By 1926 large leaps had been made in understanding quantum mechanics. Werner Heisenberg, Max Born and Pascual Jordan had published papers introducing matrix mechanics [4], and Erwin Schrödinger had invented his wave mechanics [5]. Schrödinger would later prove the equivalence of these two formalisms. Following these breakthroughs Paul Dirac proposed the Dirac equation[6] for the electron which gave a relativistic wave equation for the electron, predicting its spin property. Work also began on applying quantum mechanics to fields which would result in today's quantum field theories.

The further understanding of quantum mechanics also made it possible for new technology to emerge. Medical scanning devices are built upon principles like nuclear magnetic resonance, requiring understanding of electrons and atoms. Similarly have microscopes using the properties of electrons been able to give images of objects much smaller than the wavelength of visible light, such as the transmission electron microscope. In addition have research into semi-conductor materials enabled production of increasingly small diodes and transistors, resulting in rapid evolution of our electronics. The properties of quantum mechanics have also inspired to technological proposal of quantum computers.

Chapter 2

Quantum computing

A quantum computer makes use of quantum mechanical phenomenons which gives it different properties compared to our classical computer. By making use of these properties in a smart manner the quantum computer has the potential to solve tasks more effectively than our present day computer.

A quantum computer is also in many ways similar to a classical computer in terms of framework. It requires similar logical gates for computation and it needs quantum bits (qubits) in the same way classical computers need bits. The differences comes from the difference between quantum mechanics and classical physics. One advocate of quantum computers was Richard Feynman. in his 1982 paper[7] he argues; nature is quantum mechanical, so simulating it would require a quantum mechanical system.

2.1 The quantum bit

To understand the strengths of a quantum computer we must introduce a concept of quantum bits which utilises superposition of states. When performing measurements on a classical system one would always get the same result, given that the system was prepared in the exact same way each time. For a quantum mechanical system this will not be the case. If we have an imagined system of possible states $\{|1\rangle, |2\rangle\}$, each of these corresponding to different values of some physical quantity A. When performing measurements on the system the result would always be either A_1 or A_2, and the system would be in one of the corresponding states. For a classical system one could with certainty claim that if the measurement resulted in A_1, the system was in state $|1\rangle$ before the measurement. This is due to the limitations of the classical system; it can be in either $|1\rangle$ or $|2\rangle$.

However a quantum mechanical system will in general be in a superposition of the available states, of the form $c_1 |1\rangle + c_2 |2\rangle$. Here $|c_i|^2$ is the probability

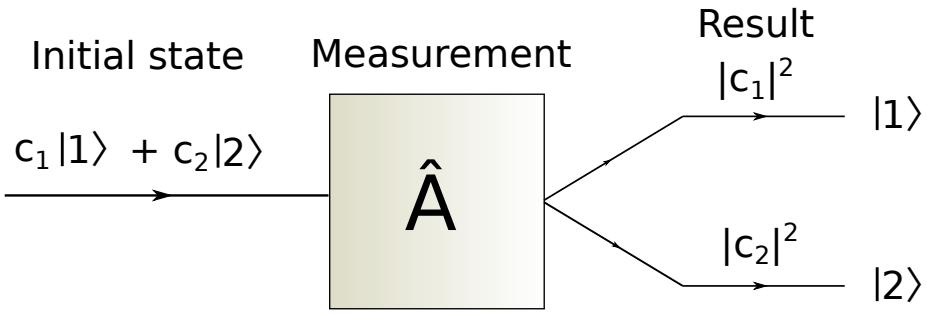

Figure 2.1: Illustration of measuring a superposition. The system if before each measurement prepared in the superposition $c_1 |1\rangle + c_2 |2\rangle$. The result of the measurement will then correspond to state $|i\rangle$ with probability $|c_i|^2$ for $i = 1, 2$

of measuring the system in state $|i\rangle$. These coefficients will be normalised such that $\sum_{i=1}^{2}|c_i|^2 = 1$. From this follows scenarios where you can prepare the system in the same superposition and measure it several times, resulting in $|1\rangle$ $|c_1|^2$ of the times and $|2\rangle$ $|c_2|^2$ of the times. This idea is illustrated in Fig.2.1. Superposition is not limited to systems of only two states, but apply for any quantum mechanical system.

Two different systems might also be quantum mechanically entangled. Say there is a system made up of two, two-level systems. Each of the systems separate might be measured and found to be in either $|1\rangle$ or $|2\rangle$. By combining these systems the space of available states of the system as a whole will expand. This means that a general state of the combined system will be in a superposition $c_{1,1} |1\rangle_1 |1\rangle_2 + c_{1,2} |1\rangle_1 |2\rangle_2 + c_{2,1} |2\rangle_1 |1\rangle_2 + c_{2,2} |2\rangle_1 |2\rangle_2$. As more systems are added the available states will increase as 2^N where N is the number of combined systems.

Two-level systems are important for quantum computing as they are used as quantum bits (qubits), the quantum mechanical equivalent to classical bits. Considering the points made about available states for many entangled two-level systems, its is evident that the amount of information stored in coefficients $c_{i,j}$ increases exponentially as the number of two-level systems increases. This prospect is one of the appealing factors of quantum computing.

Entanglement also proposes ideas for communications. Entangled states might be sent from a transmitter to a receiver in such a manner that if any third party is eavesdropping this will be detected as a change in the state, immediately telling the intended receiver that the information has been tampered with. To give an inkling of how entanglement is relevant for communication consider Fig.2.2. Two two-level systems are entangled and prepared in the state $|1\rangle_1 |1\rangle_2 + |2\rangle_1 |2\rangle_2$. Each of the two-level systems are then separated in a manner which does not affect the quantum state. By measuring either of the subsystems, which might result in $|1\rangle$ or $|2\rangle$, the state of the other subsystem is also

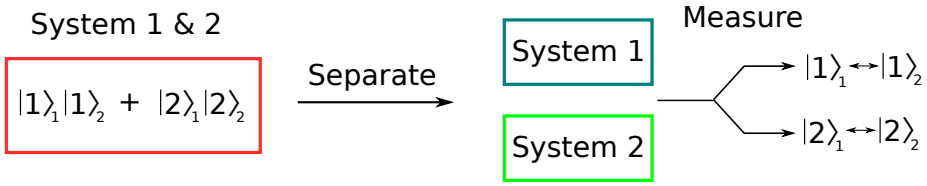

Figure 2.2: A system made up of two two-level subsystems is prepared in the superposition $|1\rangle_1 |1\rangle_2 + |2\rangle_1 |2\rangle_2$ (coefficients are here omitted). The subsystems are then separated (in a way that does not affects its state). By measuring the state of either subsystem, the state of the other subsystem is automatically given.

given by the initial state. The range of this effect has no limit.

Following the conceptual birth of quantum computers people started investigating algorithms that could run on these devices. In 1994 Peter Williston Shor proposed Shor's algorithm[8] for factorisation of integers, solving such problems much faster compared to classical algorithms for large integers. The implications of this is large due to the fact that much of the current cryptography is based on integer factorisation. Shor's algorithm have already been applied in small scale quantum computers to factorise small primes. 15 was factorised using nuclear magnetic resonance in 2001 [9] and using a photonic chip in 2009 [10] for instance.

The goal of quantum computers is to solve problems requiring computational power beyond what classical computers can offer. As the power of quantum computing comes from superposition of entangled states, it is expected to shine in problems where it can use the parallelism that stems from these superpositions. This prospect is encouraged by smart algorithms such as Shor's algorithm. A quantum computer beating classical computers in a computation is known as quantum supremacy[11]. Researchers at IBM where in 2017 able to simulate a 56-qubit quantum computer using a classical supercomputer[12], setting a provisional goal for the scales needed in order to obtain said supremacy.

2.2 Fundamental requirements to quantum bits

In order to build a quantum computer it is necessary to have qubits meeting certain criteria. David DiVincenzo summarised these in his paper 'The Physical Implementation of Quantum Computation'[13], five for computation and two for communication, and they have since been known as DiVincenzo's criteria. In this thesis only the five for computation will be considered, which are in short

1. scalability
2. initialisation

3. long coherence times
4. quantum logic gates
5. readout

These criteria are similar to what you would require from a classical bit. The strength and weaknesses of a particular two-level system will be measured by these criteria, and ultimately determine the validity of said system as a quantum bit. We will come back to these requirements when discussing two-level systems.

2.3 Physical description of two level systems

In general the Hamiltonian of a two level system can be expressed in matrix form like

$$H = a_0 \mathbb{1} + \sum_{i=1}^{3} a_i \hat{\sigma}_i \tag{2.1}$$

where $\mathbb{1}$ is the two-dimensional identity matrix and $\hat{\sigma}_i$ are the Pauli matrices. a_i are system dependent real coefficients. The units of these coefficients will be energy. This is a general representation due to the identity matrix and the Pauli matrices

$$\hat{\sigma}_1 = \begin{pmatrix} 0 & 1 \\ 1 & 0 \end{pmatrix} \quad \hat{\sigma}_2 = \begin{pmatrix} 0 & -i \\ i & 0 \end{pmatrix} \quad \hat{\sigma}_3 = \begin{pmatrix} 1 & 0 \\ 0 & -1 \end{pmatrix} \tag{2.2}$$

with real coefficients can form any Hermitian two-dimensional matrix.

Consider a general state of the two-level system $|\psi\rangle = \alpha |1\rangle + \beta |0\rangle$ where $\{\alpha, \beta\}$ are two complex numbers and $\{|1\rangle, |0\rangle\}$ are two arbitrary basis states, for instance the eigenstates of σ_3, (1,0) and (0,1).

$$|\psi\rangle = r_\alpha e^{i\phi_\alpha} |1\rangle + r_\beta e^{i\phi_\beta} |0\rangle = e^{i\phi_\alpha} \left(r_\alpha |1\rangle + r_\beta e^{i(\phi_\beta - \phi_\alpha)} |0\rangle \right) \tag{2.3}$$

Any physical measurement corresponding to this state will be of the form $\langle\psi|\hat{A}|\psi\rangle$, where $\hat{A}$ is the operator corresponding to some observable quantity A, which will cancel out any global phase of the state. It can therefore be neglected. Substitute $\phi = \phi_\beta - \phi_\alpha$

$$|\psi\rangle = r_\alpha |1\rangle + r_\beta e^{i\phi} |0\rangle = r_\alpha |1\rangle + (x + iy) |0\rangle \tag{2.4}$$

where Cartesian representation of complex numbers are used. Using the normalisation constraint we obtain

$$\langle\psi|\psi\rangle = r_\alpha^2 + x^2 + y^2 = 1 \tag{2.5}$$

which can be identified as a unit sphere by renaming $r_\alpha = z$. Representing x, y, z in polar coordinates

$$\begin{aligned} x &= r \sin\theta \cos\phi \\ y &= r \sin\theta \sin\phi \\ z &= r \cos\theta \end{aligned} \tag{2.6}$$

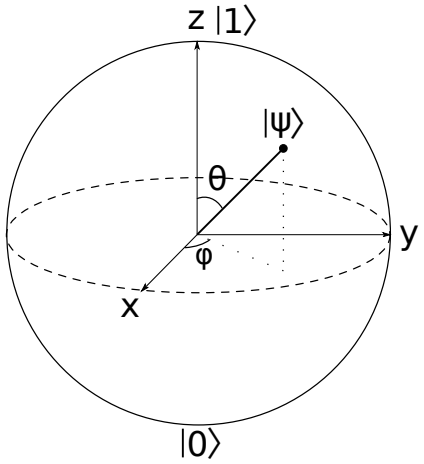

Figure 2.3: A general state $|\psi\rangle$ on the Bloch sphere with $\{\sigma_1, \sigma_2, \sigma_0 3\} \rightarrow \{\sigma_x, \sigma_y, \sigma_z\}$

the general quantum states may be expressed

$$|\psi\rangle = \cos\theta\,|1\rangle + e^{i\phi}\sin\theta\,|0\rangle \tag{2.7}$$

Looking at this expression it is evident that any state can be expressed with angles $\in [0, \frac{\pi}{2}]$. In spherical coordinates $\theta \in [0, \pi]$ so let $\theta \rightarrow \frac{\theta}{2}$ and the general state is finally

$$|\psi\rangle = \cos\frac{\theta}{2}\,|1\rangle + e^{i\phi}\sin\frac{\theta}{2}\,|0\rangle \tag{2.8}$$

This way to represent the states is known as the Bloch sphere Fig.2.3. Here the mapping $\{1, 2, 3\} \rightarrow \{x, y, z\}$ is used for the Pauli matrices (Eq.(2.2)) and $|1\rangle, |0\rangle$ are eigenstates of σ_z. Notice how $|1\rangle$ and $|0\rangle$ are anti-parallel in their Bloch sphere representation ($\theta = 0$ and $\theta = \pi$) while they are orthogonal in Hilbert space ($\langle 1|2\rangle = 0$).

The Pauli matrices can also be related to rotations in the Bloch sphere. It can be shown that

$$\begin{aligned} e^{i\phi'\hat{\sigma}_1} &= \begin{pmatrix} \cos\phi' & -i\sin\phi' \\ i\sin\phi' & \cos\phi' \end{pmatrix} \\ e^{i\phi'\hat{\sigma}_2} &= \begin{pmatrix} \cos\phi' & -\sin\phi' \\ \sin\phi' & \cos\phi' \end{pmatrix} \\ e^{i\phi'\hat{\sigma}_3} &= \begin{pmatrix} e^{-i\phi'} & 0 \\ 0 & e^{i\phi'} \end{pmatrix} \end{aligned} \tag{2.9}$$

where each of these expressions will rotate the two-level state along its respective axis in its Bloch sphere representation. By using two of these rotations one can take a state from one point on the Bloch sphere to any other point.

Following Eq.(2.9), a Hamiltonian on the form $H \propto \hat{n}\cdot\hat{\sigma} = n_1\sigma_1+n_2\sigma_2+n_3\sigma_3$ will cause a rotation along the $\hat{n}$ direction. This can be seen by solving the Schrödinger equation

$$ih\frac{\partial}{\partial t}\left|\psi\right\rangle = H\left|\psi\right\rangle \tag{2.10}$$

Since the Hamiltonian is time independent this is trivial and yields

$$\left|\psi(t)\right\rangle = e^{i\alpha\hat{n}\hat{\sigma}t}\left|\psi\right\rangle_0 \tag{2.11}$$

Where $\left|\psi\right\rangle_0$ is the initial state and α is a coefficient with terms from the Hamiltonian. The Hamiltonian will thus make the state precess along the $\hat{n}$-axis. This implies that if the Hamiltonian can be controlled, it offers rotation of the state on the Bloch sphere. This is a crucial property that will be looked closer on when considering candidate two-level systems for quantum bits.

This framework of two-level systems are applicable to any physical systems, such as electron spin, polarisation of photons and ground state and first excited state of an atom. Another point is that most physical systems have more degrees of freedom than simply two states, however if such two states are sufficiently separated from any other states they can be approximated to a two-level system.

The meaning of DiVincenzo's criteria can now be looked more into. For sufficient computational power it is necessary that the candidate two-level system can scale up by adding more and more qubits. One quantum bit working alone will not suffice. The two-level system must also have some reliable state it can be initialised into before computations are carried out, this means that for some controllable parameters the system will naturally enter this initial state. The quantum logical gates will take form as operators doing the necessary rotations on the two-level state, taking it for instance from $|0\rangle \rightarrow \frac{1}{\sqrt{2}}(|0\rangle + |1\rangle)$. These rotations can then be done sequentially to work as quantum gates corresponding to the classical logical gates. Readout methods will be based on measurable properties of the system such as energy, charge or angular momentum to determine which state the system is in.

The last criteria left is then the coherence time of states of the two-level system. The coherence time is how long an initialised state will remain well defined, and is affected by external noise. Such noise is typically related to random fluctuations in the environment of the two-level system, and will add to the system Hamiltonian, affecting the phase ϕ of the initialised state. These effects can be generalised into relaxation of the state and randomisation of the phase, both which causes loss of information, illustrated in Fig.2.4.

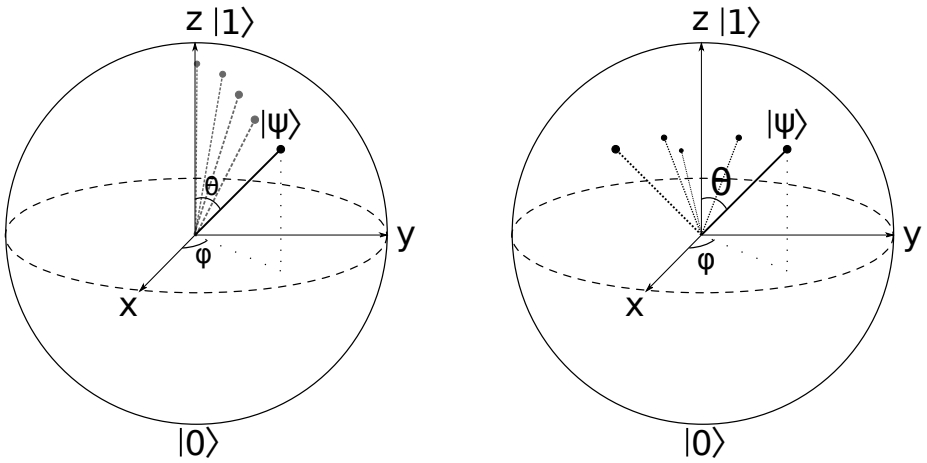

Figure 2.4: Illustration of state relaxation (left) and phase randomisation (right). Net result is loss of original quantum states and thus loss of information.

Chapter 3

Spin qubits in quantum dots

In this thesis the electron spin will be considered as a candidate quantum bit. The electron will be trapped on a quantum dot in a semi-conductor. Such systems show promise due to means of readout, initialisation, quantum logical gates and scalability, leaving the challenge of sufficient coherence times. We will look into how a quantum dot can be built and how spin qubits trapped on the dot relates to the DiVincenzo's criteria.

3.1 Quantum dots in semi-conductors

The quantum dot a region where particles trapped have practically zero degrees of spatial freedom. Particles that are sufficiently isolated from the environment will remain confined on the dot (Fig.3.1). The quantum dot that will be explored here is created in a solid, or more specifically a semi-conductor, and are used to trap electrons. The number of electrons necessary will be at most two per quantum dot for the coming considerations. It is thus sufficient to have a theoretical model for the behaviour of this number of electrons on the dot in addition to the possibility of creating said dots.

3.1.1 2-dimensional electron gas

The first directional confinement is obtained by considering electrons in the two dimensional electron gas (2DEG) created in the heterojunction between two semi-conductor materials. The 2DEG is when the energy discretisation of the electron is substantially larger in one direction opposed to the other two. The electron movement along this direction is then effectively prohibited, and the electron is confined to move in the plane spanned by remaining directions. There are several ways of realising a 2DEG such as in liquid helium [14] or if a material is inherently two-dimensional and conducting such as graphene. Here we will look closer at the high electron mobility transistor (HEMT) [15].

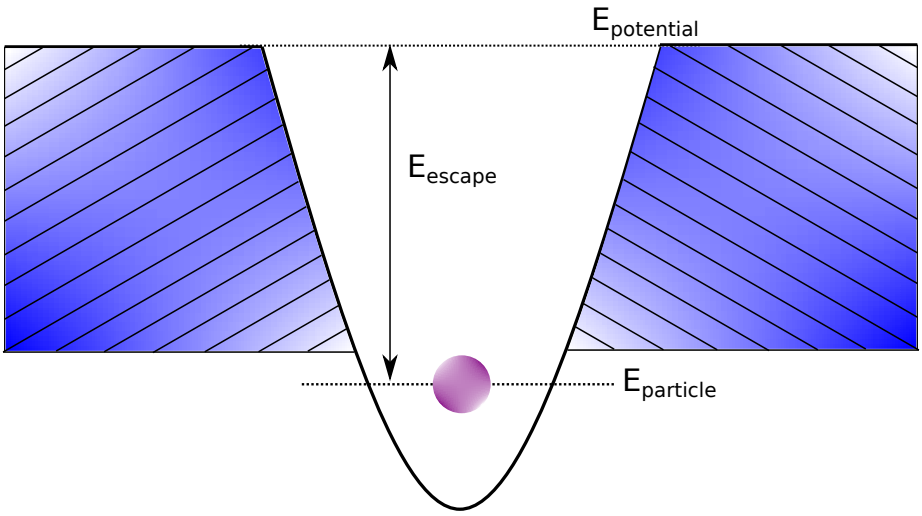

Figure 3.1: Illustration of a one-dimensional quantum dot where a particle is trapped in a harmonic like potential. The particles energy E_{particle} is lower than the confining energy $E_{\text{potential}}$. If the particle on the dot is isolated from any energy sources the particle will remain confined.

The HEMT is created with a heterojunction structure of gallium-arsenide and gallium-aluminium-arsenide (GaAs/GaAlAs) semi-conductors. It is made up of Silicone (Si) doped GaAs cap layer to protect the second Si-doped GaAlAs layer from oxidation. The third layer is undoped GaAlAs which is in junction with undoped GaAs of layer 4. This is grown on a GaAs substrate (layer 5) using for instance molecular beam epitaxy [16], to form layer by layer. The structure is illustrated, along with each layers depth, in Fig.3.2. The depths are taken from [15].

By doing this process the energy band of the HEMT will be such that in the heterojunction of GaAs/GaAlAs (layer 3 and 4) any electrons are free to move along the interface, but would require considerable energy to cross it (Fig.3.3).

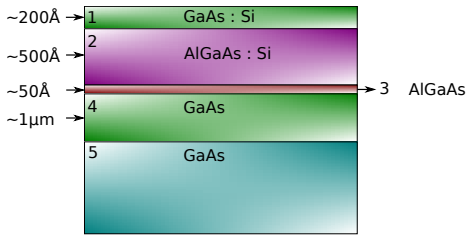

Figure 3.2: Cross section of a HEMT. The Si-doped layers are marked with : Si. This figure is the same as Figure 1 from [15]

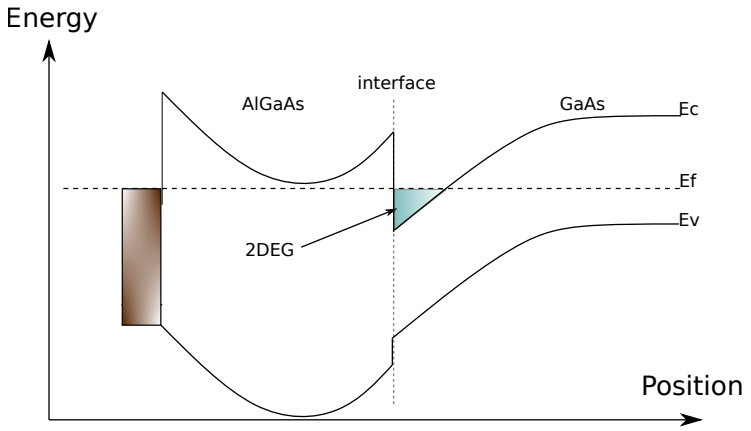

Figure 3.3: The resulting energy band of the HEMT device as a function of position in the device along the growth direction. Note the triangular well in the interface where the 2DEG foRMS. These energy bands can also be seen in Figure 5(a) in [15]

This is then effectively a 2DEG.

3.1.2 Nanolithograpy

Electron confined in the 2DEG are further confined through etching gates on top of the heterostructure through nanolithography [17]. These gates can be made in any geometrical form which creates a potential landscape in the 2DEG accordingly. In Fig.3.4 three sets of gates have been etched on top of the heterostructure. Pair 1 and 3 determine the tunnelling of electrons to and from the dot while pair 2 determine the electrostatic energy of electrons on the dot.

These quantum dots where initially used as artificial atoms [18], and efforts where put into creating a transport theory for electrons on them. Electrons on the dot where shown to behave similarly to electron orbiting the nucleus in atoms, and filling schemes for the quantum dots for large number of electrons was worked out. For the purpose of using the quantum dots as qubits it is however enough to consider just one or two electrons on a given quantum dot.

To use the spin of electrons as the quantum bit it is necessary to trap the exact needed number of electrons on the dot through adjusting the voltage over the gates in Fig.3.4. In order to achieve this there must be a theoretical framework which describes when and how electrons may enter and leave the dot, taking into account the number of electrons already on the dot. Since we only need a small number of electrons the constant-interaction model (CI) is sufficient to describe electron transport through the dot [18].

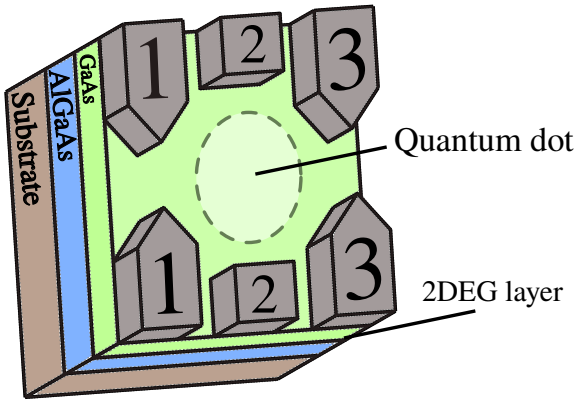

Figure 3.4: Three pairs of gates are made through nanolithography on top of the heterostructure to produce a confining potential landscape within the 2DEG. Pair 1 and 3 control the tunnelling to and from the dot. Pair 2 control the electrostatic energy of electrons on the dot.

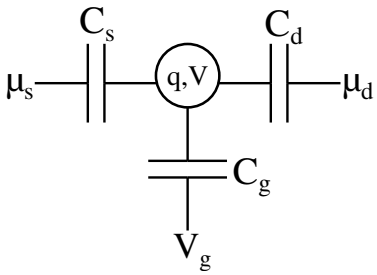

Figure 3.5: Diagram representing the capacitance which relates to the gates on the heterostructure Fig.3.4.

3.1.3 Quantum dot electron transport

The constant-interaction model (CI) assumes that the quantum levels and the number of electrons are independent. Further it is assumed that the Coulomb interaction between electrons on the dot and between dot electrons and electrons in the environment is parameterised by a capacitance C, which is independent of the number of electrons on the dot. This capacitance is then $C = C_s + C_d + C_g$ where C_s (C_d) represents the capacitance between dot and source (drain) and C_g between dot and the gate potential (Fig.3.5). With these approximations the energy of an N electron dot is

$$U(N) = [e(N - N_0) - C_g V_g]^2/2C + \sum_N E_{n,l}(B) \tag{3.1}$$

N_0 is the number of electrons on the dot for $V_g = 0$. $C_g V_g$ is the induced charge on the dot from the gate voltage V_g through the gate capacitance C_g. The last term sums the energy contribution $E_{n,l}$ from the orbital states occupied by the electrons.

The electrochemical potential μ is defined as the energy associated with adding another electron to the dot and given by

$$\begin{aligned} \mu(N) &= U(N) - U(N-1) \\ \mu(N) &= (N - N_0 - 1/2)e^2/C - e(C_g/C)V_g + E_N \end{aligned} \tag{3.2}$$

Where E_N is the orbital energy of electron number N. Adding another electron comes with a higher electrochemical potential. This change is known as the addition energy

$$\Delta\mu(N) = \mu(N+1) - \mu(N) = e^2/C + \Delta E \tag{3.3}$$

Where $\Delta E = E_{N+1} - E_N$. If they both occupy the same orbital $\Delta E = 0$ and only the Coloumb energy $E_C = e^2/C$ will contribute. For our applications any excited orbital states will be assumed out of reach, as they will be much larger in energy compared to what is available in the system.

These consideration are then enough to discuss the transport of electrons through the dot. Electrons residing in each part of the 2DEG will have a different electrochemical potential. These parts are the source, drain and the dot itself. Lets assumed the dot is initially empty and denote the electrochemical potential of the dot as μ. The condition for current through the dot is then $\mu_{\text{source}} > \mu > \mu_{\text{drain}}$, and current will not flow if $\mu > \mu_{source}, \mu_{\text{drain}}$. The last part is known as the Coulomb blockade. These conditions can be seen in Fig.3.6

Since it is the spin of electrons that are the candidate two-level system let us make some remarks relating it to the electrochemical potential. In the absence of any magnetic field the electrochemical potential of an electron with spin-up is equal to an electron with spin-down and thus if one electron enters the dot it can have any orientation of its spin. This is due to the Zeeman energy E_Z related

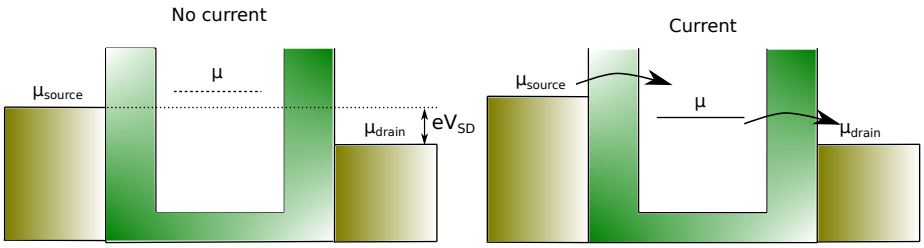

Figure 3.6: Two different cases of the electrochemical potential μ. On the left the the system is in Coulomb blockade. On the right the condition for current to flow is met, $\mu_{\text{source}} > \mu > \mu_{\text{drain}}$. The source and drain are related by the external voltage $\mu_{\text{source}} - \mu_{\text{source}} = eV_{SD}$

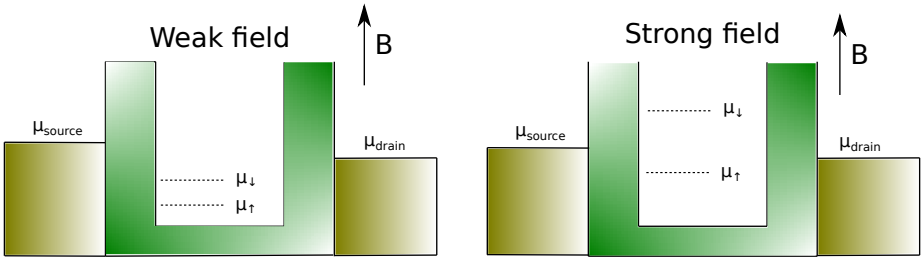

Figure 3.7: Difference between $\mu_\uparrow$ and $\mu_\downarrow$ for strong and weak magnetic fields

to the spin is $\propto B$. Adding an external magnetic field across the dot will then separate the electrochemical potential of spin-up and spin-down. This effect might be small such that $\mu_\uparrow \simeq \mu_\downarrow$ and both might be within the condition for electron entering the dot. If however the magnetic field is of sufficient strength the splitting can be large enough so that only one of the spin-orientation is eligible for entering the dot (Fig.3.7).

3.2 Single-spin quantum bit

The single-spin quantum bit uses the different spin-states, $\{|\uparrow\rangle, |\downarrow\rangle\}$, of an electron as logical states. The single electron will be trapped on the dot, and the dot will subsequently be in the Coulomb blockade such that no flow of electrons are possible. A magnetic field can then be applied over the dot, lifting the degeneracy of the $|\uparrow\rangle$ and $|\downarrow\rangle$ states, with resulting spin Hamiltonian

$$H = g\mu_B \vec{B} \cdot \vec{S} = \frac{g\mu_B \hbar}{2} \sum_i B_i \sigma_i \tag{3.4}$$

with σ_i being the Pauli matrices (Eq.(2.2)), g is the g-factor of the material, μ_B is the Bohr magneton and $\hbar$ is Planck's reduced constant. Let us do the

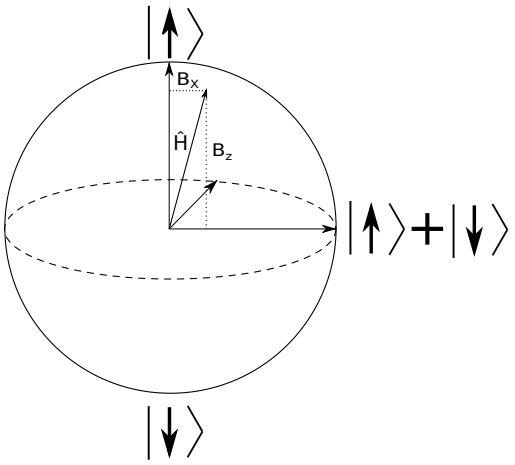

Figure 3.8: The Bloch sphere of the single-spin system. The effective field of the Hamiltonian is given by $\hat{H}$, here taken without any y-component to the magnetic field.

mapping $\{1,2,3\} \rightarrow \{x,y,z\}$ and assume that the spin is quantised in the z-direction, such that $\{|\uparrow\rangle, |\downarrow\rangle\}$ are eigenstates of σ_z. Writing out the sum of the Hamiltonian gives

$$H = \frac{g\mu_B\hbar}{2}\begin{pmatrix} B_z & B_x - iB_y \\ B_x + iB_y & -B_z \end{pmatrix} = \frac{g\mu_B\hbar}{2}\begin{pmatrix} B_z & B_- \\ B_+ & -B_z \end{pmatrix} \tag{3.5}$$

Where (B_+, B_-) relates to the spin raising/lowering operators $S_\pm = S_x \pm iS_y$. These operators connects the two spin states, $S_+ |\downarrow\rangle \propto |\uparrow\rangle$ and $S_- |\uparrow\rangle \propto |\downarrow\rangle$.

The Bloch sphere of this system is shown in Fig.3.8. Applying a magnetic field along the logical axis (z-direction) will cause precession of the spin-state along this axis, and similarly for applying a magnetic field along the $|\uparrow\rangle + |\downarrow\rangle$ axis (x-direction).

Using single-spin quantum bits was originally proposed by Daniel Loss and David P. DiVincenzo in 1998 [19]. The idea of using quantum dots in semiconductors was motivated by the inherent scalability of such devices. Their proposal included two coupled single-spin dots where the additional dot was needed to implement the necessary quantum logical gates. One of the dots would also be coupled to an auxiliary ferromagnetic dot to allow for single-qubit operations. Note that each dot still only would hold one electron, which separates this setup from the double-spin quantum dot.

Qubit-qubit interaction could be implemented in nearby quantum dots, such as the two in the double-dot device shown in Fig.3.9. The gate pairs 2,4 and 6 sets up a barrier potential between each region, determining the tunnelling, and the voltages set the Coulomb energy of electrons on the dots. If each dot

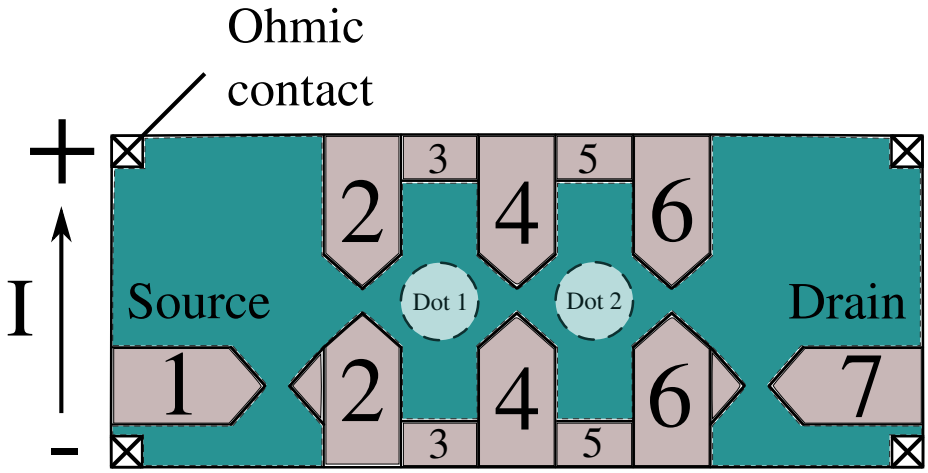

Figure 3.9: Schematic of the double dot device. Gate pair 1 and 7 creates two quantum point contacts which are used as electrometers to detect charge. Pair 2 determines tunnelling between source and dot 1, pair 4 tunnelling between the dots and pair 6 tunnelling between dot 2 and drain. Pair 3 and 5 determine the electrostatic energy of electrons on the dots.

contains exactly one electron and if the tunnel coupling is small compared to the charging energy on the dots the interaction can be expressed

$$H_S(t) = J\vec{S}_1 \cdot \vec{S}_2 \tag{3.6}$$

with $J = 4t^2/u$ where u is the charging energy and t is the tunnelling coefficient. The dots are tuned such that u is equal for both dots and is the energy that must be overcome for one electron to tunnel to the other dot. This interaction would then lead to implementation of the exclusive OR gate (XOR) which along with single-qubit operations can be made to do any quantum computation [20].

Initialisation of the system is possible applying a sufficiently strong magnetic field such that the electrochemical potential of electrons with spin up and down are split, where one is above the electrochemical potential of the source and one is below. This is similar to the situation outlined in Fig.3.7. By doing this only one of the spin-states will be allowed to enter the dot.

Readout can be performed by measuring the charge on the dot through a quantum point contact. The method relies on the Zeeman-energy of the two spin states to sufficiently split the electrochemical potentials $\mu_\uparrow$ and $\mu_\downarrow$, such that $\mu_\downarrow > \mu_{\text{source}} > \mu_\uparrow$. If the electron have spin-down it will tunnel out of the dot and another electron with spin-up will tunnel into the dot. In the opposite case where the electron have spin-up it will remain on the dot. See Fig.3.10. These two cases will cause different response from the quantum point contact (gate 1).

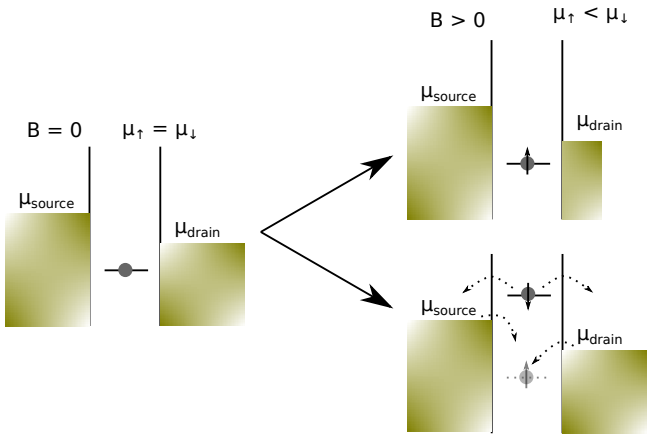

Figure 3.10: Readout of the quantum dot. The magnetic field is set to $B = 0$ initially and the spin of the electron on the dot can be either up or down. Applying a magnetic field will cause $\mu_\downarrow > \mu_{\text{source}}, \mu_{\text{source}} > \mu_\uparrow$. If the electron have spin-down it will tunnel out of the dot and an electron with spin-up will tunnel into the dot.

As the spins are controlled through magnetic fields (Eq.(3.5)) the system is vulnerable to noise in the magnetic fields. Any sources of noise will enter into the Hamiltonian and start rotating the state in a random manner, causing dephasing and loss of information. This decoherence is a result of the electrons interaction with the environment as it travels through the semi-conductor. There are two particular interactions that is important for the coherence times of the electron spin in semi-conductors, namely spin-orbit interaction and hyperfine interaction, both which are relativistic corrections to the Hamiltonian. Before summarising the single-spin quantum dot we will look into these two effects.

3.2.1 Spin-orbit interaction

The spin-orbit interaction (SOI) has its name from the magnetic field experienced by an electron orbiting a nucleus. This internal magnetic field is proportional to the electric field from the positively charges nucleus and the momentum of the electron. An electron travelling through a solid will experience the electric field from the atoms on the lattice. There are primarily two sources of net contribution to the SOI.

One of these contributions come from bulk inversion asymmetry present in the zinc-blende structure of GaAs. This effect is known as the Dresselhaus contribution [21]. The strong confinement in the growth direction, here taken as the z-direction, leads to the effective expression in leading order of p

$$H_D = \beta[-p_x\sigma_x + p_y\sigma_y] \tag{3.7}$$

where β depends on material properties and $\langle p_z^2 \rangle$, which is much larger than the corresponding terms in x- and y-direction. $\{\sigma_x, \sigma_y\}$ correspond to the previously mentioned Pauli matrices $\{\sigma_1, \sigma_2\}$ (Eq.(2.2)).

The other source of SOI contribution is electric fields originating from asymmetric confining potentials, which is present in the GaAs/AlGaAs interface. This effect is knows as the Rashba term [22] and is of the form

$$H_R = \alpha(-p_y\sigma_x + p_x\sigma_y) \tag{3.8}$$

with α is material specific and also includes the effect of the confining potential.

This spin-orbit Hamiltonian $H_{SO} = H_D + H_R$ will cause a net rotation of the electron spin as it travels through the 2DEG. A quantity corresponding to a rotation of π is called the spin-orbit length l_{SO}. For electrons travelling through the 2DEG in GaAs experiments have measured l_{SO} to the order $\sim \mu$m [23]. Since a quantum dot is typically of size $\sim$ 100nm, much smaller than l_{SO}, the effect of SOI is expected to be relatively slow working. The the inverse relaxation time have been shown to vary $T_1^{-1} \in [1, 1000]s^{-1}$ for magnetic fields $B \in [1, 7]$T [24]. These effects are dominated by the SOI, but relaxation is also in principled affected by the hyperfine interaction (Sec 3.2.2).

The time scale for phase randomisation T_2 will always be less than the relaxation time T_1. This is due to a relaxation of the state will inevitably include a loss of the phase. However to leading order of in SOI there is no pure phase randomisation, and $T_1 = T_2$ [25].

3.2.2 Hyperfine interaction

Hyperfine interaction (HI) follows from the electron spin interacting with the spin of a nucleus through the hyperfine coupling. For an electron in a semiconductor the spin will interact with many nuclear spins in the material. This many nuclei interaction can be expressed [26]

$$H_{HF} = \sum_k^N A_k \hat{I}_k \hat{S} \tag{3.9}$$

where the sum is over all the nuclei the electron interacts with. $\hat{I}_k$ is the spin operator of nucleus k and $\hat{S}$ the spin operator of the electron. The coupling strength A_k will in generally vary as it is proportional to the overlap between their respective wave functions.

If we neglect any quantum mechanical effects, such as entanglements between nuclear and electron spin, HI may be treated semi-classically. The main notion of this being a valid approach is the electron-spin dynamics being rapid compared to the nuclear-spin dynamics. The HI then takes the form

$$H_{HF} = g\mu_B \vec{B}_N \hat{S} \tag{3.10}$$

where

$$g\mu_B \vec{B}_N = \sum_k^N A_k \langle \hat{I}_k \rangle \tag{3.11}$$

Which treats the nuclear spins as a contribution to some net magnetic field affecting the electron.

For GaAs the nuclear field will have a maximum value, corresponding to parallel alignment of all nuclei, of 5T [27]. This number is independent of how many nuclei the electron overlaps with. If the number of nuclei N increases, the contribution from each nucleus to the nuclear field will be smaller. The typical coupling strength goes as $A_K \propto 1/N$.

In the absence of external field the net nuclear field will on average be zero, with fluctuations around the average value. This is due the nuclear magnetic moment is so small, such that even for very small temperature the nuclear Zeeman splitting is below the thermal energy of the system. As a result the nuclear spins will have no preferred direction and orient randomly. These fluctuations will be of order $\frac{1}{\sqrt{N}}$ [28] corresponding to field of the order mT for quantum dots with $N \approx 10^6$, resulting in both the direction and magnitude of the magnetic field evolving randomly in time. Assuming that that these random field values are drawn from a Gaussian distribution the dephasing time T_2 is given by [29]

$$T_2 = \frac{\hbar\sqrt{2}}{g\mu_B \sqrt{\langle (B_N^Z \rangle)^2}} \tag{3.12}$$

with results of order 10ns for $\sqrt{\langle (B_N^Z \rangle)^2}$ ∼mT.

Relaxation of a single-spin qubit requires finite coupling to the $\hat{S}^{\pm}$ by the environment. For the case of HI, we see that this corresponds to having non-zero $B_N^{x,y}$. However, it turns out that hyperfine-induced relaxation rates are typically much lower than the rates caused by SOI. The main effect from HI is therefore qubit dephasing.

There are some additional factors regarding HI worth mentioning. Since it depends on overlap between nuclear and electron wave functions, only s orbitals electrons will have substantial contribution. p orbitals have very little overlap with the nuclei. In our considerations all electrons will however be s orbitals. Another aspect is that the semi-conductor material might have components of zero nuclear spin nuclei. Thus $B_N \to B_N(1-x)$ where x is the fraction of zero nuclear spin nuclei. Silicone for instance have an abundance of ^{28}Si (92.2%) where this isotope have no nuclear spin. Thus a semi-conductor made out of Silicone and further purified can achieve $x \simeq 1$.

3.2.3 Summary of the single-spin quantum bit

Having briefly discussed interactions between the electron spin and the semiconductor environment it is evident that coherence times will be a large chal-

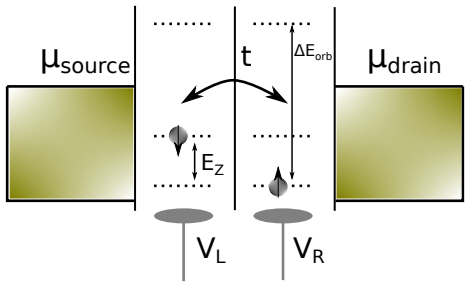

Figure 3.11: Schematic of the double dot. Any excited orbital states are out of reach for the electrons. The local voltages $\{V_L, V_R\}$ can be tuned to affect the Coulomb energy on the dot. The spin-states are separated by some external magnetic field.

lenge due to HI. To overcome this, qubit operations must happen at timescales well below T_2. Operating the single-spin qubit in itself relies on using highly localised magnetic fields. Tuning these magnetic fields on such low timescales and localised on individual dots is practically very difficult.

The first step in improving this is to devise a system where the magnetic operation of the qubit states can be exchanged with electric operation. Managing this would solve one of the issues present to the single-spin qubit. Proposals in this direction involve systems with multiple spins and dots

3.3 Double-spin quantum bit

The qubit is here made out of two electrons and two quantum dots. The electrons can either be on separate dots or doubly occupy one of the dots through tunnelling from one dot to the other. It is assumed that the energy scale of the system is such that any excited orbitals are out of reach for the electrons. This is illustrated in Fig.3.11. The double dot gate patterns are similar to the ones in Fig.3.9.

Assuming each dot is limited to a maximum number of $N = 2$ electrons the Coulomb part of the Hamiltonian can be expressed

$$H_C = \frac{1}{2}\sum_i U_i N_i(N_i - 1) - eV_i N_i + U' N_1 N_2 \tag{3.13}$$

Here U_i is the charging energy of dot i and U' is the nearest neighbour charging energy. Additionally there is some energy related to the local potentials V_i for each of the dot. This model, when adding the tunnel coupling, is known as the Hubbard model and used to describe the transport through the double dot [30].

Eq.(3.13) gives rise to a two dimensional charge stability diagram (Fig.3.12). The diagram shows the energetically favoured electron configurations for differ-

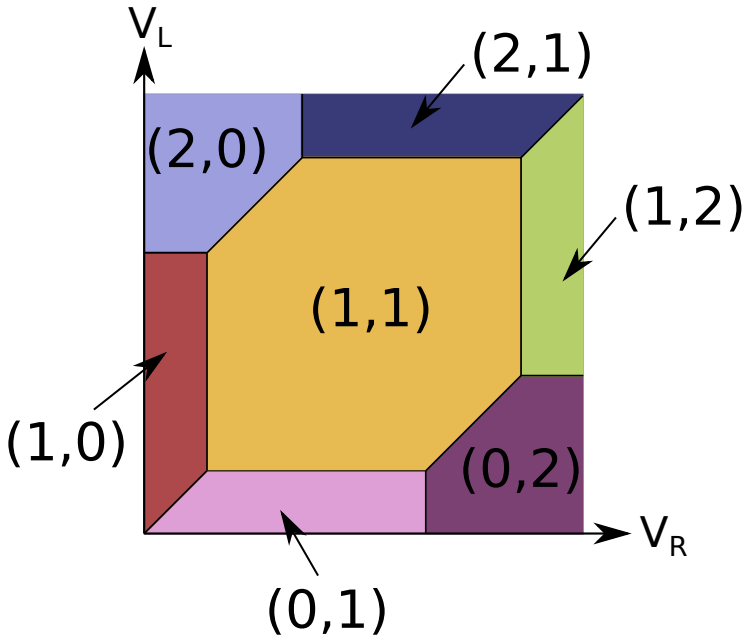

Figure 3.12: Charge stability diagram for the double dot as a functions of $\{V_L, V_R\}$. The maximum number of electrons on each dot is limited to two.

ent applied voltages and which configurations it is possible to transitions between. These transitions can happen along the black lines between the different regions where the Coulomb energy of each configuration is degenerate. This is the equivalent to the occupancy numbers discussed for the single-spin quantum dot with the constant interaction model. Since the total number of electrons is set to $N = 2$ the regions of interest are $(2,0) \leftrightarrow (1,1) \leftrightarrow (0,2)$. By choice the system will be tuned at the crossing $(1,1) \leftrightarrow (0,2)$.

A consequence of adding another dot is increasing the number of states available in the system. One way to express the states, with the given restrictions, is $\{|\uparrow_1\uparrow_2\rangle, |\uparrow_1\downarrow_2\rangle, |\downarrow_1\uparrow_2\rangle, |\downarrow_1\downarrow_2\rangle, |02\rangle\}$. Electrons are fermions and must therefore obey the Pauli exclusion principle, that is the wave function must be anti-symmetric with respect to particle exchange. Since any excited orbitals are outside of reach for the system energy, this implies that for the $|02\rangle$ state the anti-symmetry must lie in the spin part of the wave function. The two-particle state meeting this requirement is the singlet state $|S\rangle = \frac{1}{\sqrt{2}}(|\uparrow\downarrow\rangle - |\downarrow\uparrow\rangle)$

This invites for a convenient choice of basis

$$\begin{aligned}
|S\rangle &= \frac{1}{\sqrt{2}}(|\uparrow_1\downarrow_2\rangle - |\downarrow_1\uparrow_2\rangle) \\
|T\rangle_0 &= \frac{1}{\sqrt{2}}(|\uparrow_1\downarrow_2\rangle + |\downarrow_1\uparrow_2\rangle) \\
|T\rangle_+ &= |\uparrow_1\uparrow_2\rangle \\
|T\rangle_- &= |\downarrow_1\downarrow_2\rangle \\
|02\rangle &= |0S\rangle
\end{aligned} \tag{3.14}$$

with the subscript denoting which dot. T here stands for triplet. From this it is clear that the tunnelling between the dots only connects the $|S\rangle$ and $|0S\rangle$ states. Assuming that there is an external magnetic field $\vec{B} = B_0\hat{z}$ and any interaction with the environment can be neglected, the total Hamiltonian of the system can be expressed on matrix form

$$H = \begin{pmatrix} -E_Z & 0 & 0 & 0 & 0 \\ 0 & E_Z & 0 & 0 & 0 \\ 0 & 0 & 0 & 0 & 0 \\ 0 & 0 & 0 & 0 & t \\ 0 & 0 & 0 & t & u-\epsilon \end{pmatrix} \tag{3.15}$$

where the Coulomb energy of the (1,1) states are shifted out. $\epsilon = -V_L + V_R$ and $u = U - U'$ which will for simplicity be neglected. The energies and corresponding states of this Hamiltonian is then

$$\begin{aligned}
E_S^{\pm} &= -\frac{\epsilon}{2} \pm \sqrt{\left(\frac{\epsilon}{2}\right)^2 + t^2} \\
|E_S^+\rangle &= \cos\frac{\theta}{2}|S\rangle + \sin\frac{\theta}{2}|0S\rangle \\
|E_S^-\rangle &= \sin\frac{\theta}{2}|S\rangle - \cos\frac{\theta}{2}|0S\rangle \\
\tan\theta &= \frac{t}{(\epsilon/2)}
\end{aligned} \tag{3.16}$$

These energies are plotted in Fig.3.13

Consider the $\{|S\rangle, |T\rangle_0\}$ states in Fig.3.13. As the external field is increased, these states will be further separated from $\{|T\rangle_+, |T\rangle_-\}$. If the system is tuned in the regime $\epsilon \ll 0$, the doubly occupied singlet state $|0S\rangle$ will also be largely separated in energy from the the mentioned states. In this regime the system can then be considered as a two-level system with basis $\{|S\rangle, |T\rangle_0\}$ where the effects from the remaining three states are considered perturbations.

The Hamiltonian of this two-level system can then be written

$$H = -\frac{J(\epsilon)}{2}\mathbb{1} - \frac{J(\epsilon)}{2}\sigma_z + \Delta B_z\sigma_x = \begin{pmatrix} -J(\epsilon) & \Delta B_z \\ \Delta B_z & 0 \end{pmatrix} \tag{3.17}$$

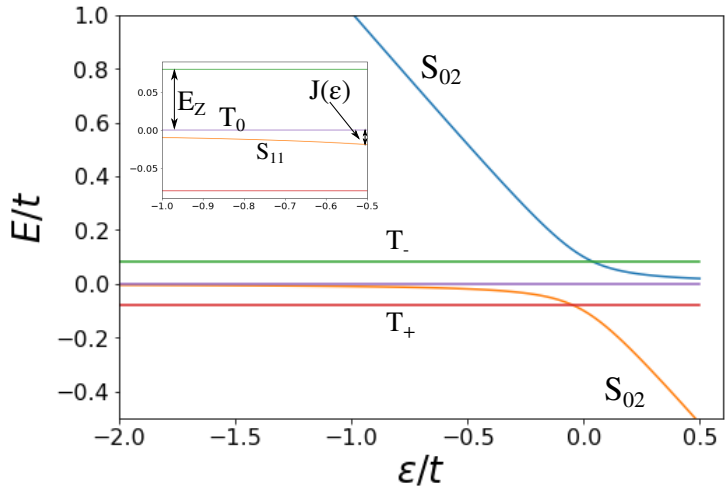

Figure 3.13: The energy spectrum of the double-spin quantum dot in the absence of spin-interaction. $\epsilon \propto -V_L + V_R$, E_Z is the Zeeman splitting due to an external magnetic field. For this plot $\frac{E_Z}{t} = 0.8$

Where $J(\epsilon) \approx \frac{t^2}{|\epsilon|}$ and $\Delta B_z = B_z^1 - B_z^2$ is the gradient field between the dots caused by effective nuclear fields.

Let these two states define a qubit. Rotations along the logical axis can then be controlled by tuning ϵ in the regime where $J(\epsilon) \gg \Delta B_z$. Similarly if $J(\epsilon) \ll \Delta B_z$ the Hamiltonian will cause rotations along the $\frac{1}{\sqrt{2}}(|S\rangle + |T\rangle_0)$ axis. This is then called a ST-qubit and the axes are illustrated in Fig.3.14

The ST-qubit have been demonstrated experimentally with logic operation with a gating time of order 180ps [31], well below the dephasing time caused by hyperfine interaction. The system can be initialised in the $|0S\rangle$ state and swept adiabatically to the limit $J(\epsilon) \ll \Delta B_z$. Here the state will assume the ground state of $|\uparrow\downarrow\rangle, |\downarrow\uparrow\rangle$. From here on operations can be performed to rotate the qubit along the directions needed by rapidly tuning ϵ.

The challenge with this setup are the random nuclear fields affecting the dot. As the system will relax into on of the $|\uparrow\downarrow\rangle, |\downarrow\uparrow\rangle$ states, which of them is the ground state will be random depending on positive or negative ΔB_z. Seeing however that there is established electrical control over one of the axes progress has been made from the single-spin qubit. The next step is then to add yet another spin along with an additional dot.

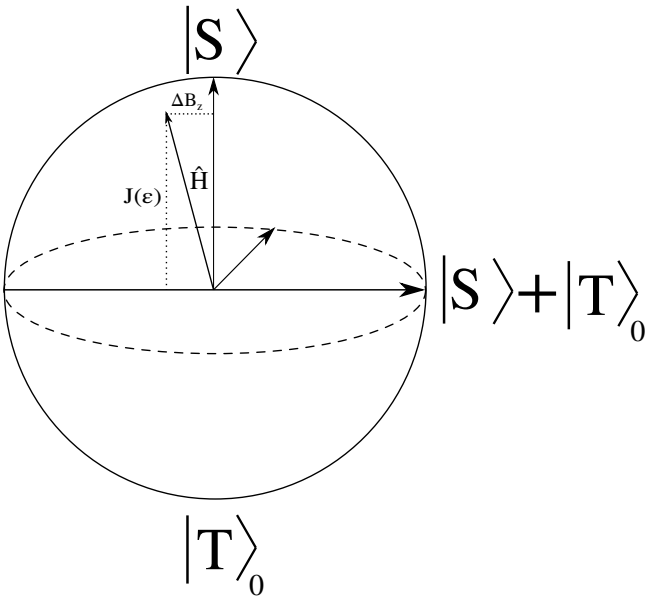

Figure 3.14: Bloch sphere for the ST-qubit. The effective field from the Hamiltonian $\hat{H}$ is indicated. Note that the signs of $J(\epsilon)$ and ΔB_z are chosen arbitrarily for this illustration.

3.4 Triple-spin quantum bit

The triple-spin quantum bit is a natural continuation of the double-spin quantum bit and similar considerations will be made as before. As the name suggests the number of electrons in the system is increased to three with equal amounts of quantum dots. Electrons may tunnel between each of the dots $1 \leftrightarrow 2 \leftrightarrow 3$ generally with different tunnelling strengths. For the following discussions the tunnelling strengths will be assumed equal $t_{12} = t_{23} = t$ and only nearest neighbour tunnelling is possible, $t_{13} \simeq 0$. Further are any excited orbital states out of reach for the system energy such that the maximum number of electrons $N = 2$ for each dot. This is illustrated in Fig.3.15 and a sample gate pattern is provided in Fig.3.16.

The Hubbard model will again be used [32] which provides the Coulomb part of the Hamiltonian

$$H_C = \frac{U}{2}\sum_i N_i(N_i - 1) - eV_iN_i + U'\sum_{\langle i,j\rangle} N_iN_j \tag{3.18}$$

with N_i being the number of electrons on dot i, V_i is the associated potential, U' is the charging energy and $\langle i, j\rangle$ denotes a sum over nearest neighbours.

Eq.(3.18) provides the charge stability diagram of the triple-spin quantum dot, provided in Fig.3.17. Along the axes are $V_{\mathrm{m}} = \frac{eV_1+eV_3}{2} - eV_2$ and $\epsilon =$

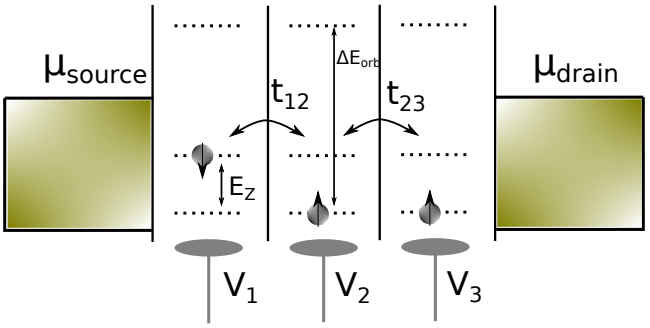

Figure 3.15: The triple-spin quantum bit. Electrons can tunnel between each of the dots. The energy related to any excited orbital states are larger than the energy scale of the system. Each dot has an associated voltage gate which determines the Coulomb energy of the dot.

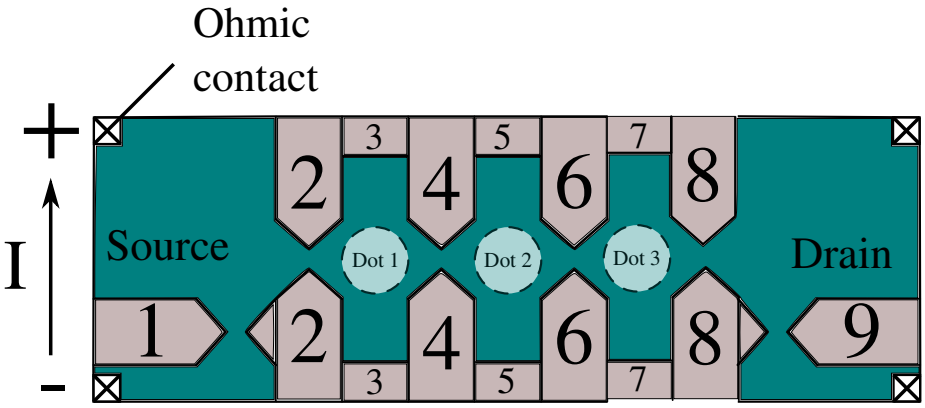

Figure 3.16: Schematic of the triple dot device. Gate pair 1 and 9 creates two quantum point contacts which are used as electrometers to detect charge. Pair 2 determines tunnelling between source and dot 1, pair 4 and 6 tunnelling between the dots and pair 8 tunnelling between dot 3 and drain. Pair 3, 5 and 7 determine the electrostatic energy of electrons on the dots.

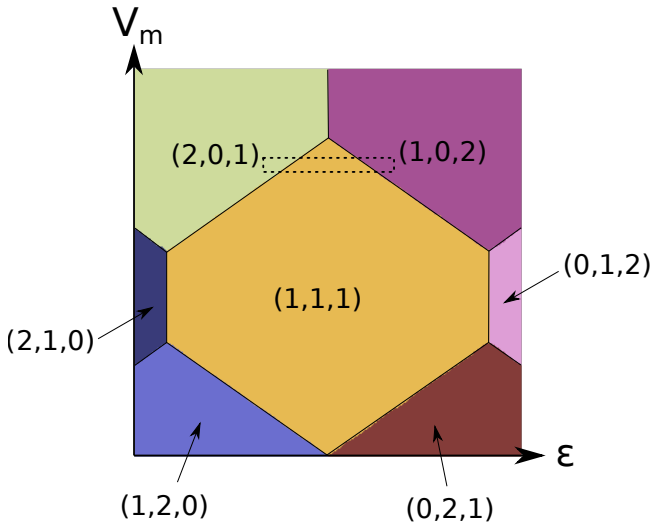

Figure 3.17: Charge stability diagram of the triple-spin quantum dot. $V_{\mathrm{m}} = \frac{V_1+V_3}{2} - V_2$ and $\epsilon = \frac{V_3-V_1}{2}$. $V_{\mathrm{tot}} = \sum_i V_i$ is held constant.

$\frac{eV_3-eV_1}{2}$. In the following expressions the electron charge $e = 1$ for brevity. This diagram is with the restriction of total number of electrons in the system $N = 3$. The system will be tuned in the region $(2,0,1) \leftrightarrow (1,1,1) \leftrightarrow (1,0,2)$ indicated by the dashed box.

Adding the third electron and dot comes along with yet more complex states for the system. In the assigned region of tuning the number of states available are now twelve. Four of them comes from the double occupied states. These states will with the same reasoning as for the double-spin quantum dot be of the form (1,0,S) and (S,0,1), where the single electron can have either spin-up or spin-down. The spin-orientation of the single electron thus determines which spin-subspace the doubly occupied states reside in, which can be $S_z = \pm\frac{1}{2}$.

In the absence of any spin-flip terms in the Hamiltonian, interaction can only happen between states in their respective spin-subspace. With a strong external magnetic field these sub-spaces will be split up in energy due to the Zeeman-splitting. Let us for now then focus on the $S_z = \frac{1}{2}$ sub-space. By choosing the basis

$$\begin{aligned}
|Q_{1/2}\rangle &= \frac{1}{\sqrt{3}}(|\uparrow\uparrow\downarrow\rangle + |\uparrow\downarrow\uparrow\rangle + |\downarrow\uparrow\uparrow\rangle) \\
|D_T\rangle &= \frac{1}{\sqrt{6}}(|\uparrow\uparrow\downarrow\rangle - 2\,|\uparrow\downarrow\uparrow\rangle + |\downarrow\uparrow\uparrow\rangle) \\
|D_S\rangle &= \frac{1}{\sqrt{2}}(|\uparrow\uparrow\downarrow\rangle - |\downarrow\uparrow\uparrow\rangle) \\
&|\uparrow 0S\rangle\,,\ |S0\uparrow\rangle
\end{aligned} \tag{3.19}$$

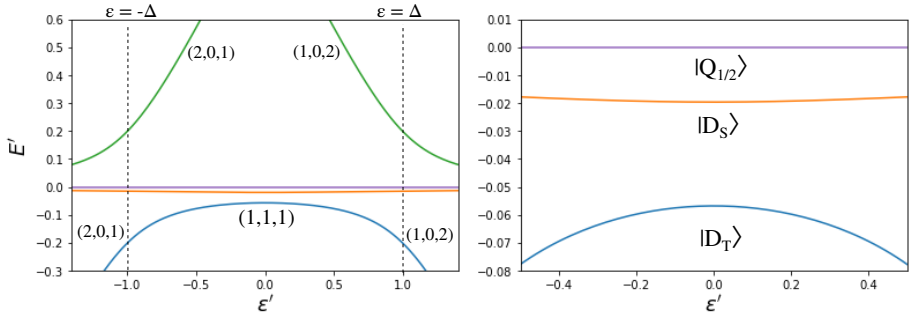

Figure 3.18: Energy spectrum of the triple dot Hamiltonian (3.20). $E' = \frac{E}{\Delta}$. $\epsilon' = \frac{\epsilon}{\Delta}$. The regions are marked to show which electron distribution is favourable. For these plots $\frac{t}{\Delta} = 0.2$

the Hamiltonian can be expressed in matrix form as

$$H = \begin{pmatrix} 0 & 0 & 0 & 0 & 0 \\ 0 & 0 & 0 & \frac{t}{2} & \frac{t}{2} \\ 0 & 0 & 0 & -\frac{\sqrt{3}t}{2} & \frac{\sqrt{3}t}{2} \\ 0 & \frac{t}{2} & -\frac{\sqrt{3}t}{2} & \Delta+\epsilon & 0 \\ 0 & \frac{t}{2} & \frac{\sqrt{3}t}{2} & 0 & \Delta-\epsilon \end{pmatrix} \tag{3.20}$$

where the Coulomb energy $E_C = -V_{\text{tot}} + 2U'$ of the (1,1,1) states are shifted out. $\Delta = U - U' - V_{\text{m}}$ and $\epsilon = \frac{V_3 - V_1}{2}$.

The Hamiltonian (3.20) can be solved numerically to get the energy spectrum of the system, which is given in Fig.3.18. The right part shows a zoom in around $\epsilon = 0$ where the states is to a good approximation equal to $|D_S\rangle$ and $|D_T\rangle$. This can be understood based on the large energy differences to the coupled doubly occupied states $|\uparrow 0S\rangle, |S0\uparrow\rangle$, and the numerically solved states coefficients in Fig.3.19 confiRMS this.

Considering the rightmost part of Fig.3.18 a candidate for the logical basis $\{|0\rangle, |1\rangle\}$ is $\{|D_T\rangle, |D_S\rangle\}$. Performing a Schrieffer-Wolf transformation to first order (see also Sec 4.1) in $\frac{t}{\Delta}$, the effective two-level Hamiltonian can be written [33]

$$H = -\frac{1}{2}\begin{pmatrix} 3J(\epsilon) & \sqrt{3}j(\epsilon) \\ \sqrt{3}j(\epsilon) & J(\epsilon) \end{pmatrix} = -\left(2J(\epsilon)\mathbb{1} + J(\epsilon)\sigma_z + \sqrt{3}j(\epsilon)\sigma_x\right) \tag{3.21}$$

with

$$\begin{aligned} J(\epsilon) &= \frac{t^2}{2}\left(\frac{1}{\Delta+\epsilon} + \frac{1}{\Delta-\epsilon}\right) \\ j(\epsilon) &= \frac{t^2}{2}\left(\frac{1}{\Delta-\epsilon} - \frac{1}{\Delta+\epsilon}\right) \end{aligned} \tag{3.22}$$

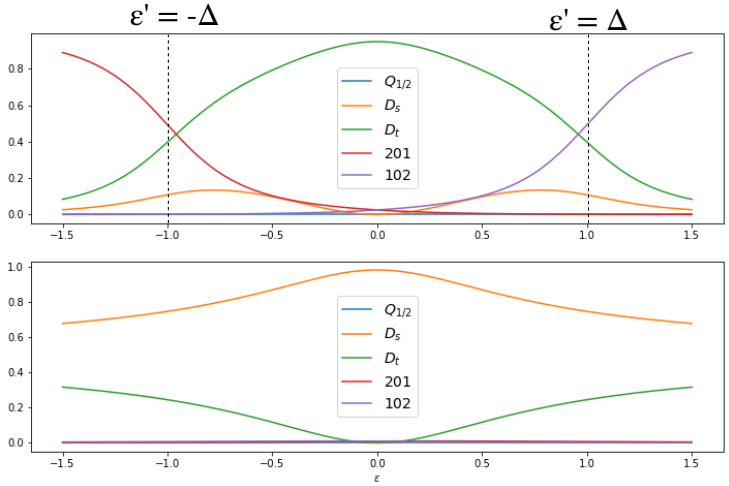

Figure 3.19: State coefficients squared for the two lowest lying energy states in Fig.3.18. The upper plot is for the lowest energy and the lower plot is for the second lowest energy level.

and σ_z, σ_x being the Pauli matrices, Eq.(2.2), used previously.

The direction of the effective field from the Hamiltonian is given by

$$\tan\theta = \frac{\sqrt{3}j(\epsilon)}{J(\epsilon)} \tag{3.23}$$

which have maximum angle for the limits

$$\lim_{\epsilon\to\pm\Delta}\theta(\epsilon) = \pm\frac{\pi}{3} = \pm 60^\circ \tag{3.24}$$

shown in Fig.3.20. With these two axes of control the Hamiltonian can be used to apply any set of rotations on the Bloch sphere. The problem of magnetic control from the single-spin and double-spin quantum dot is then resolved. Experiments have shown that is form of control is indeed achievable [34][33].

The limits in these experiments are the short coherence times in relation to the HI. This is caused by the gradient fields between the dots, which can be seen by looking at H_{nuc} [33]

$$\begin{pmatrix} -\frac{1}{3}(\Delta B_{12}-\Delta B_{23}) & -\sqrt{\frac{1}{3}}(\Delta B_{12}+\Delta B_{23}) & -\sqrt{\frac{2}{3}}(\Delta B_{12}+\Delta B_{23}) \\ -\sqrt{\frac{1}{3}}(\Delta B_{12}+\Delta B_{23}) & \frac{1}{3}(\Delta B_{12}-\Delta B_{23}) & -\frac{\sqrt{2}}{3}(\Delta B_{12}-\Delta B_{23}) \\ -\sqrt{\frac{2}{3}}(\Delta B_{12}+\Delta B_{23}) & -\frac{\sqrt{2}}{3}(\Delta B_{12}-\Delta B_{23}) & 0 \end{pmatrix} \tag{3.25}$$

In the $\{|0\rangle, |1\rangle, |Q_{1/2}\rangle\}$ basis. $\Delta B_{ij} = B_i^z - B_j^z$. So the HI can cause both leakage into the $|Q_{3/2}\rangle$ state and add fluctuations to the two-level Hamiltonian.

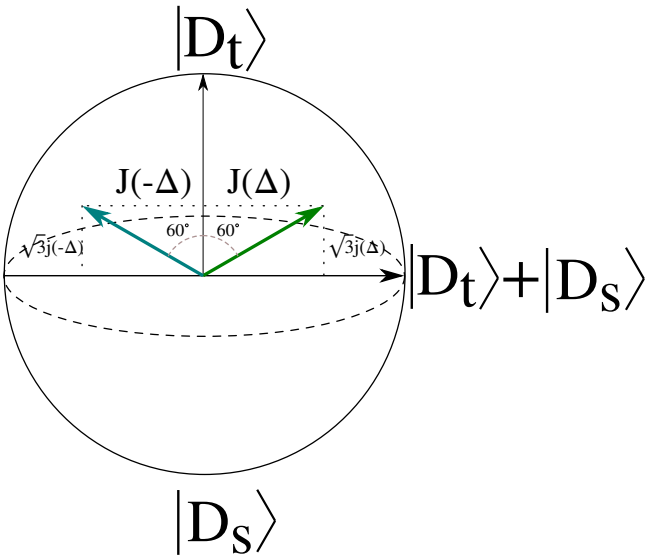

Figure 3.20: The Bloch sphere for the triple-spin quantum dot. The effective fields from the Hamiltonian is shown in the case of $\lim \epsilon \to \pm\Delta$.

The energy spacing between $|Q_{3/2}\rangle$ and the logical basis can be controlled through the tunnelling coupling and such be made sufficiently large compared to the HI between them. The problem remaining is to suppress the effect from these random fluctuations and by doing so increase the coherence time of the system.

There are a few proposals for solving this issue. One is to use a semi-condutor of purified silicone (Si) such that the zero nuclear spin isotope ^{28}Si makes out $> 99\%$ of the material [35][36]. Another proposal is to make use of the spin from four electrons in a quadruple dot where there exists a two-level subspace insensitive to the nuclear field gradients [37].

A third way is to devise a procedure for controlling these nuclear fields in the three dots, and find a way to actively suppress the fluctuations. In this thesis will attempt this by inducing spin-flips in such a way to reduce or otherwise remove the randomness of ΔB_{ij}. The goal is to perform such a procedure on time scales much lower than the natural relaxation time nuclear spin such that computations might be performed while the system is in a 'controlled' configuration.

The plan is to use Landau-Zener transitions (See Sec 4.2) that force spin-flips in one of the dots, depending on the precise electron wave function. Thus a feedback mechanism is created, hopefully making the nuclear field gradients control themselves.

Chapter 4

Theoretical basics

Before discussing the model for nuclear field dynamics in Section 5 we will introduce theoretical concepts which are necessary for later use.

4.1 First order Schrieffer-Wolff transformation

Consider a Hamiltonian

$$H = H_0 + V \tag{4.1}$$

where H_0 have known eigenstates $|m\rangle$ with corresponding energy E_m, and V is considered a small perturbation causing a coupling t between the eigenstates $|m\rangle$. Further it is also assumed V only have off-diagonal entries. This last assumption can always be made true by having H_0 absorb potential diagonal elements $\langle m|\, V\, |m\rangle$ from V.

The idea is then to find a unitary transformation $\tilde{H} = e^S H e^{-S}$ such that $\tilde{H}$ is diagonal to first order in t. The generator S of this transformation will be of same order as V. Expand the expression and make use of V being a small perturbation

$$\tilde{H} \approx [1 + S + \frac{1}{2}S^2](H_0 + V)[1 - S + \frac{1}{2}S^2] \tag{4.2}$$

By collecting all the terms and neglecting all terms $\sim t^3$ and using the commutator $[A, B] = AB - BA$ the expression can be rewritten

$$\tilde{H} \approx H_0 + V + [S, H_0] + [S, V] + \frac{1}{2}[S, [S, H_0]] \tag{4.3}$$

Since we want an expression for the Hamiltonian that is diagonal up to order t any first order terms must cancel out. This is obtained by putting $[S, H_0] = -V$. The resulting expression becomes

$$\tilde{H} = H_0 + \frac{1}{2}[S, V] + \mathcal{O}(t^3) \tag{4.4}$$

Make use of the assumption that H_0 only contains diagonal terms $H_{0,ii} = E_i$, which results in the following component form of the commutator $[S, V]$

$$[S, H_0]_{ij} = S_{ik}H_{0,kj} - H_{0,ik}S_{kj} = S_{ij}E_j - E_iS_{ij} = -V_{ij} \tag{4.5}$$

solving this for S_{ij} then gives

$$S_{ij} = \frac{V_{ij}}{E_i - E_j} \tag{4.6}$$

Inserting this into Eq.(4.4) gives the final expression on component form to order t^2

$$\tilde{H}_{ij} = H_{0,ij} + \frac{1}{2}V_{ik}V_{kj}\left(\frac{1}{\Delta E_{ik}} + \frac{1}{\Delta E_{jk}}\right) \tag{4.7}$$

with ΔE_{ij} being the energy difference between unperturbed states $|i\rangle$ and $|j\rangle$

4.2 Landau-Zener transition

The Landau-Zener transition attempts to describe the linear sweeping of one energy level through another in the presence of a coupling between the levels. This scenario can be described by the Hamiltonian

$$H = \begin{pmatrix} 0 & q \\ q & E(t) \end{pmatrix} \tag{4.8}$$

in the basis $|\psi\rangle_1, |\psi\rangle_2$ which are the eigenstates of H for $q \to 0$. Here E_1 the energy of $|\psi\rangle_1$ is set as zero and $E_2 = E(t)$ is the energy of $|\psi\rangle_2$.

This system can be solved analytically to yield

$$\begin{aligned} E_\pm &= \frac{E(t)}{2} \pm \sqrt{\left(\frac{E(t)}{2}\right)^2 + q^2} \\ |E_+\rangle &= \cos\frac{\theta}{2}|S\rangle + \sin\frac{\theta}{2}|0S\rangle \\ |E_-\rangle &= \sin\frac{\theta}{2}|S\rangle - \cos\frac{\theta}{2}|0S\rangle \\ \tan\theta &= \frac{t}{(E(t)/2)} \end{aligned} \tag{4.9}$$

which shows that the coupling q between the states lead to admixture of them and an anti-crossing at $E(t) = 0$.

Looking at limiting values where $|E(t)| \gg 0$ we can see how the admixture state behaves compared to the uncoupled system. Let us consider $|E_+\rangle$

$E(t) > 0:$	$E(t) < 0:$
$E_+ \simeq E(t)$	$E_+ \simeq \frac{q^2}{\lvert E(t\rvert} \simeq 0$
$\lvert E_+\rangle \simeq \lvert\psi\rangle_2$	$\lvert E_+\rangle \simeq \lvert\psi\rangle_1$

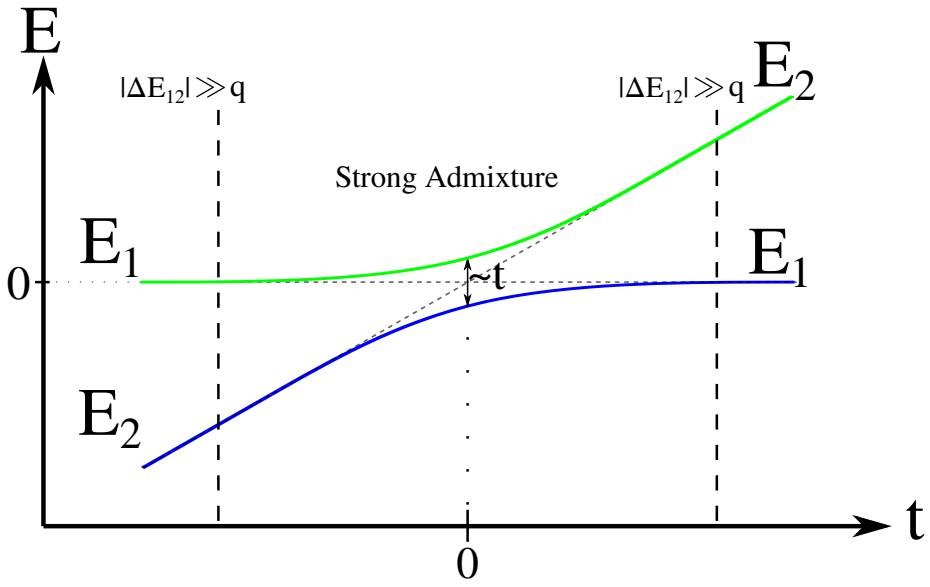

Figure 4.1: The energies of Eq.(4.9). The dashed line show energy without any coupling.

and opposite for $|E_-\rangle$. So far away from the crossing the system will act equivalent to an uncoupled system. The minimum separation is at the anti-crossing where $\Delta E_{+-} = E_+ - E_- \sim q$. Close to the crossing the admixture between $|\psi\rangle_1$ and $|\psi\rangle_2$ is large. This is illustrated in Fig.4.1 where a linear $E(t)$ is used.

If the system is initialised in the $|\psi\rangle_1$ at a time far away from the crossing point, what is the probability that we will end up in $|\psi\rangle_2$ at a later time also far away from the crossing point by slowly sweeping through the crossing. 'Far away' means that the energy separation is large compared to the coupling $|E_1 - E_2| \gg q$ and 'slowly' compares to the slope $|\frac{\partial}{\partial t}(E_1 - E_2)|$.

By assuming that the energy crossing $|E_1 - E_2| \propto t$ and that the coupling q is independent of time $\frac{\partial q}{\partial t} = \dot{q} = 0$ this probability is given by

$$\begin{aligned} P &= 1 - e^{-2\pi\gamma} \\ \gamma &= \frac{t^2}{\hbar v} \end{aligned} \tag{4.10}$$

where $v = |\frac{\partial}{\partial t}(E_1(t) - E_2(t)|$ is the effective sweeping speed through the crossing. Eq.(4.10) is known as the Landau-Zener transition probability [38].

Chapter 5

Landau-Zener transitions in the TQD

The main goal of this thesis is to control the nuclear gradient fields of the TQD. This is proposed to do with $|Q_{3/2}\rangle \leftrightarrow |0\rangle$ Landau-Zener transitions since the crossing between these states can be controlled by applying an external magnetic field. Such processes are expected to increase the coherence time of the system, specifically the time related to dephasing of the quantum state. By controlling the fields the contribution from H_{nuc} Eq.(3.25) can be considered a constant effect instead of randomly fluctuating. Improvement of the coherence times can also be obtained by reducing the magnitude of the nuclear field fluctuations, which can be considered an alternative goal.

5.1 $Q_{3/2}$-D_t crossing without hyperfine interaction

The system in consideration is the triple-spin quantum dot with Hubbard Hamiltonian [32]

$$H = \sum_{i=1}^{3} \frac{U}{2} n_i(n_i - 1) - V_i n_i + E_z S_i^z + \sum_{<i,j>} U_c n_i n_j + \left(t_{ij} c_{i,\sigma}^\dagger c_{j,\sigma} + t_{ij}^* c_{j,\sigma}^\dagger c_{i,\sigma} \right) \tag{5.1}$$

U is the charging energy of a single dot, U_c is the charging energy between dots, V_i is the potential over dot i, $t_{ij} = t$ is the coupling between dot i and j. $c_{j,\sigma}^\dagger$ ($c_{j,\sigma}$) creates (destroy) an electron on dot j with spin σ.

By including the $|Q_{3/2}\rangle = |\uparrow\uparrow\uparrow\rangle$ state with $S_z = \frac{3}{2}$ and ignoring for now the

nuclear fields, the Hamiltonian can be expressed on matrix form

$$H = \begin{pmatrix} E_Z & 0 & 0 & 0 & 0 & 0 \\ 0 & 0 & 0 & 0 & 0 & 0 \\ 0 & 0 & 0 & 0 & \frac{t}{2} & \frac{t}{2} \\ 0 & 0 & 0 & 0 & -\frac{\sqrt{3}t}{2} & \frac{\sqrt{3}t}{2} \\ 0 & 0 & \frac{t}{2} & -\frac{\sqrt{3}t}{2} & \Delta+\epsilon & 0 \\ 0 & 0 & \frac{t}{2} & \frac{\sqrt{3}t}{2} & 0 & \Delta-\epsilon \end{pmatrix} \tag{5.2}$$

The energy have been shifted such that $|Q_{1/2}\rangle$ is defined as zero energy and where $E_Z = g\mu_B B_z$ is the Zeeman energy. This is expressed in the basis

$$\begin{aligned} |Q_{3/2}\rangle &= |\uparrow\uparrow\uparrow\rangle \\ |Q_{1/2}\rangle &= \frac{1}{\sqrt{3}}(|\uparrow\uparrow\downarrow\rangle + |\uparrow\downarrow\uparrow\rangle + |\downarrow\uparrow\uparrow\rangle) \\ |D_T\rangle &= \frac{1}{\sqrt{6}}(|\uparrow\uparrow\downarrow\rangle - 2\,|\uparrow\downarrow\uparrow\rangle + |\downarrow\uparrow\uparrow\rangle) \\ |D_S\rangle &= \frac{1}{\sqrt{2}}(|\uparrow\uparrow\downarrow\rangle - |\downarrow\uparrow\uparrow\rangle) \\ |\uparrow 0S\rangle,\ &|S0\uparrow\rangle \end{aligned} \tag{5.3}$$

The energy spectrum is similar to before with the addition of $|Q_{3/2}\rangle$, Fig.5.1. The crossing points between $|Q_{3/2}\rangle$ and $|0\rangle$ can be changed by tuning the magnetic field. The method applied will be to initialise in the ground state 'far away' from the crossing point, and sweep ϵ through the crossing. 'Far away' here means that the energy difference between the states are much larger than the minimal separation at the crossing.

$|0\rangle \leftrightarrow |Q_{3/2}\rangle$ can happen through Landau-Zener transitions, which are in different spin sub-spaces $S_z = \frac{1}{2}$ and $S_z = \frac{3}{2}$. We assume then that a nuclei have flipped in a opposite manner. Sweeping these states through their crossing many times will effect on the nuclei polarisation and can be compared to how the polarisation behaves without these forced transitions. As the polarisation changes so will the crossing point between the states, and subsequently the form of the electron wave function. This will in turn affect the transition probability of each sweep and a feedback cycle is established.

The mechanism behind these spin-flips is the hyperfine interaction between electron spin and the nuclear spin. The detailed explanation for the TQD is given in Sec 5.2, here we will write the final expression for the TQD coupling in $\{|Q_{3/2}\rangle, |0\rangle\}$ subspace

$$\begin{aligned} H_{HF} = H^+_{HF} + H^-_{HF} &= \begin{pmatrix} 0 & q_+ \\ q_+^* & 0 \end{pmatrix} + \begin{pmatrix} 0 & q_- \\ q_-^* & 0 \end{pmatrix} \\ q_\pm^2 &= \frac{A^2}{N}\left(\frac{1\pm P_1}{2}|\gamma_0|^2 + \frac{1\pm P_2}{2}|\beta_0|^2 + \frac{1\pm P_3}{2}|\alpha_0|^2\right) \end{aligned} \tag{5.4}$$

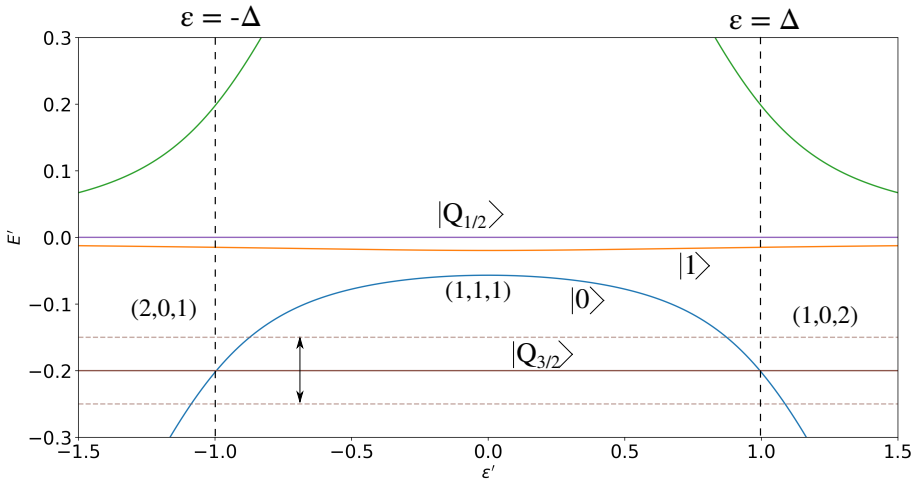

Figure 5.1: Energy spectrum where $|Q_{3/2}\rangle$ is added in. The axes are scaled with Δ. The crossing point between $|0\rangle$ and $|Q_{3/2}\rangle$ depends on the Zeeman energy, illustrated by the dashed line above and below $|Q_{3/2}\rangle$

where q_+ relates to $|0\rangle \rightarrow |Q_{3/2}\rangle$ and q_- to $|Q_{3/2}\rangle \rightarrow |0\rangle$. The coefficients $\{\alpha_0, \beta_0, \gamma_0\} = \{\alpha(\epsilon_c), \beta(\epsilon_c), \gamma(\epsilon_c)\}$ comes from the form of $|0\rangle$

$$|0\rangle \sim \alpha(\epsilon)\,|\uparrow\uparrow\downarrow\rangle + \beta(\epsilon)\,|\uparrow\downarrow\uparrow\rangle + \gamma(\epsilon)\,|\downarrow\uparrow\uparrow\rangle \tag{5.5}$$

where $\epsilon = \epsilon_c$ is the crossing point between the energies, which changes as the polarisation changes.

Keeping this feedback mechanism in mind we will start by investigating numerically different sweep procedures and look at the response in the polarisation. These procedures are illustrated in Fig.5.2-5.5

As we shall see some of the sweep procedures investigated turns out to suppress the nuclear gradient field fluctuations. With this in mind we wish to get a more detailed understanding of the dynamics by deriving an analytic expression for all spin-flip rates. In Sec 5.4 we take the first steps towards this by deriving an expression for all wave functions included, valid for any ϵ.

5.2 Hyperfine interaction in TQD

We have previously looked at the general mechanism behind the hyperfine interaction (HI) in Eq.(3.9). Here we seek to find the explicit expression of HI for the $\{|Q_{3/2}\rangle, |0\rangle\}$ subsystem. The resulting coefficients can be applied in the Landau-Zener formula Eq.(4.10) to determine the transition probabilities.

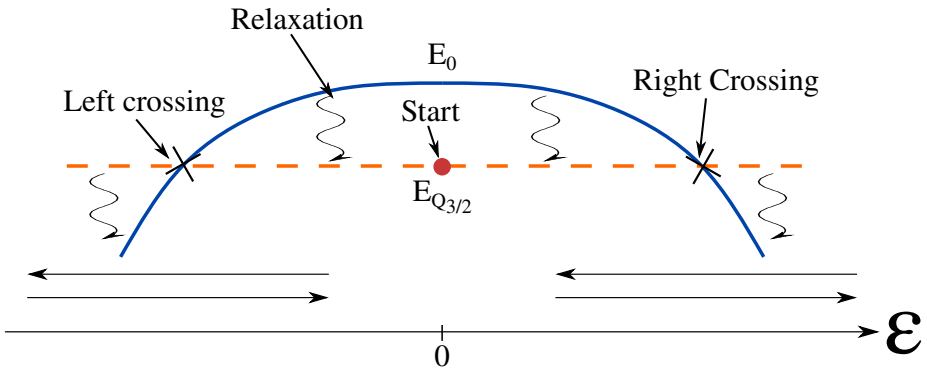

Figure 5.2: Begin at $\epsilon = 0$ in the $|Q_{3/2}\rangle$ state. Relaxation into ground state after each crossing. Alternate between right and left crossing.

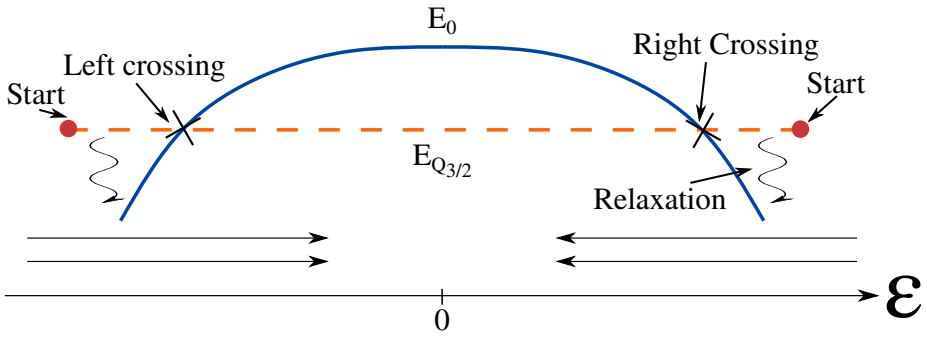

Figure 5.3: Begin at $|\epsilon| > \Delta$ in the $|0\rangle$ state. Go through the crossing. Alternate between beginning at left and right side.

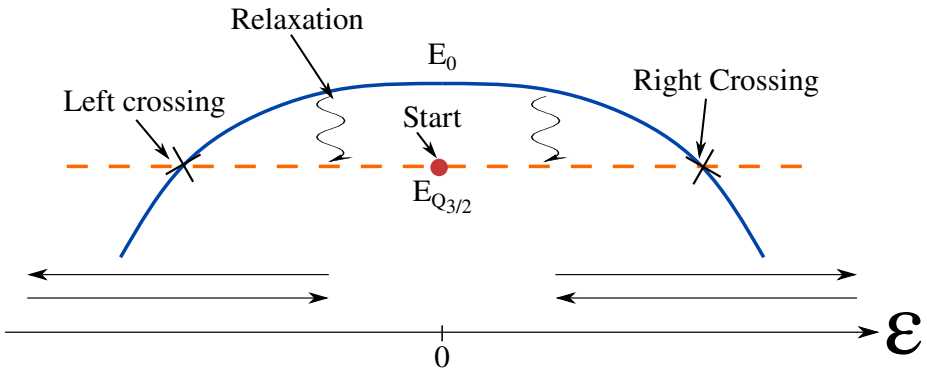

Figure 5.4: Begin at $\epsilon = 0$ in the $|Q_{3/2}\rangle$ state. Relaxation into ground state only in the regime $|\epsilon| < \Delta$. Alternate between right and left crossing.

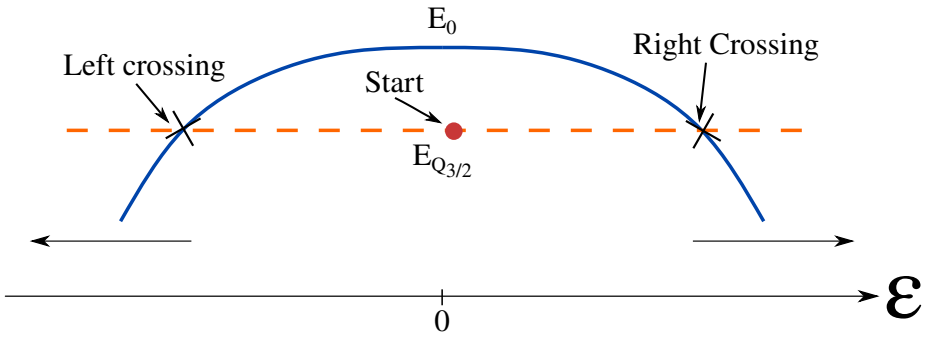

Figure 5.5: Begin at $\epsilon = 0$ in the $|Q_{3/2}\rangle$ state. Alternate between sweeping left and right.

Begin with the initial expression

$$H_{HF} = \sum_{i,n} A_{in} \hat{I}_n \hat{S}_i = \sum_{i,n} A_{in} \left(\frac{\hat{I}_n^+ \hat{S}_i^-}{2} + \frac{\hat{I}_n^- \hat{S}_i^+}{2} + \hat{I}_n^z \hat{S}_i^z \right) \tag{5.6}$$

where lowering and raising operators have been used in the last expression (see Eq.(3.5)). The sum goes over all N nuclei on each dot i. Let us focus on the $\hat{S}_i^+$ and restrict ourselves to one dot for brevity. Further we will assume spin-1/2 nuclei.

$$H_{HF}^+ = \sum_n A_n \frac{\hat{I}_n^- \hat{S}^+}{2} \tag{5.7}$$

where $A_n = A\nu|\psi(\vec{r}_n)|^2$. $A \sim (10^{-5} - 10^{-4})$eV [39] being a material property, ν is the size of the unit cell and $\psi(\vec{r})$ is the electron spatial wave function at position $\vec{r}$. $\vec{r}_n$ is the position of nuclei n. Assuming for simplicity that the $\psi(\vec{r})$ is constant over the dot volume, Fig.5.6. This gives

$$A_n = A\nu|\psi(\vec{r}_n)|^2 = A\nu\frac{1}{V} = \frac{A}{N} \tag{5.8}$$

and inserted into the operator

$$H_{HF}^+ = \frac{A}{N} \sum_n \frac{\hat{I}_n^- \hat{S}^+}{2} \tag{5.9}$$

From here on will the quantum mechanical properties of the nuclei be neglected, and the effect from the nuclear spins considered merely an effective field acting on the electron spin. In doing so each single nuclei is not so interesting, but rather how many of them can join in a spin-flip process. This number is equal to the amount of nuclei with spin oriented up, denoted by N^+.

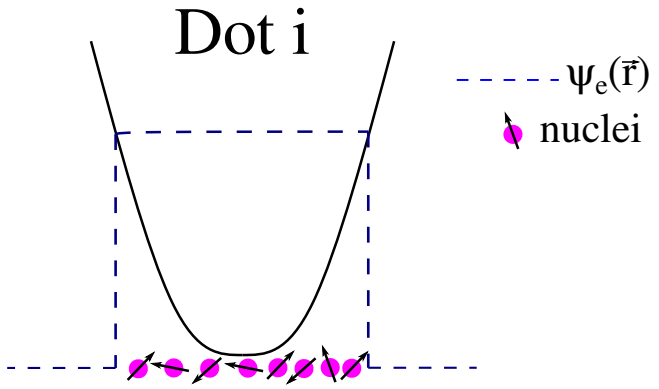

Figure 5.6: Illustration of the constant electron spatial wave function over a dot. The electron will only interact with the N nuclei on the dot.

Consider then initial states $|i\rangle$ and final states $|f\rangle$ of the form

$$\begin{aligned} |i\rangle &= |0\rangle_e \, |N^+\rangle_n \\ |f\rangle &= |Q_{3/2}\rangle_e \, |\dots \downarrow_j \dots\rangle_n \end{aligned} \tag{5.10}$$

such that all N^+ different final states connects to the same initial state. e denotes electron part and n denotes the nuclear part. Each of these couplings will be of the form

$$\langle f|H^+_{HF}|i\rangle = \frac{A}{N} \langle Q_{3/2}|\hat{S}^+|0\rangle \tag{5.11}$$

or in matrix form

$$\begin{pmatrix} E_i & \frac{A}{N_i} \langle Q_{3/2}| \hat{S}^+_i |0\rangle & \frac{A}{N_i} \langle Q_{3/2}| \hat{S}^+_i |0\rangle & \dots \\ \frac{A}{N_i} \langle Q_{3/2}| \hat{S}^+_i |0\rangle^* & E^1_f & 0 & \dots \\ \frac{A}{N_i} \langle Q_{3/2}| \hat{S}^+_i |0\rangle^* & 0 & \ddots & \dots \\ \vdots & \vdots & \vdots & \ddots \end{pmatrix} \tag{5.12}$$

We assume that all final states energy are the same $E^j_f = E_f$.

These contributions can be put together into one effective coupling corresponding to spin-flip in the dot. Disregarding the exact final spin configuration of the nuclear spin ensemble, we can write the 'total' matrix element as

$$\langle f|H^+_{HF}|i\rangle = \frac{A}{N}\sqrt{N^+} \langle Q_{3/2}|\hat{S}^+|0\rangle \tag{5.13}$$

Let us introduce the total number of nuclei $N = N^+ + N^-$ and the polarisation $P = \frac{N^+ - N^-}{N}$. N^+ can then be expressed

$$N^+ = N\frac{1+P}{2} \tag{5.14}$$

Insert into the effective coupling Eq.(5.13) and obtain

$$\langle f|H^{+}_{HF}|i\rangle = \frac{A}{\sqrt{N}}\sqrt{\frac{1+P}{2}}\,\langle Q_{3/2}|\hat{S}^{+}|0\rangle \tag{5.15}$$

with corresponding final state

$$|f\rangle = |Q_{3/2}\rangle_e\,|N^{+}-1\rangle_n \tag{5.16}$$

This procedure was for one of the three dots. The different nuclear states of he dots do not overlap, causing them to be fully uncoupled. This leads to three effective states, one for each dot, coupling to the final state. These three states can again be combined in a similar fashion as done for the N^{+} different states for one dot. This results in the effective coupling between final state and spin-flip in any dot, and takes the form

$$\langle \tilde{f}|H^{+}_{HF}|i\rangle = \frac{A}{\sqrt{N}}\sqrt{\sum_i \frac{1+P_i}{2}|\langle Q_{3/2}|\hat{S}^{+}_i|0\rangle\,|^2} \tag{5.17}$$

Where it is assumed that all dots have the same number of nuclei N. This is then the necessary matrix element for Landau-Zener transitions Eq.(4.10). The corresponding final state is

$$|\tilde{f}\rangle = \mathcal{N}\sum_i \sqrt{\frac{1+P_i}{2}}(|\langle Q_{3/2}|\hat{S}^{+}_i|0\rangle\,|)\,|Q_{3/2}\rangle_e\,|N^{+}_i-1\rangle \tag{5.18}$$

with $\mathcal{N}$ a normalisation constant

The probability p_j for the spin-flip to have happened in dot j is then given by

$$p_j = \frac{\frac{1+P_j}{2}|\langle Q_{3/2}|\hat{S}^{+}_j|0\rangle\,|^2}{\sum_i \frac{1+P_i}{2}|\langle Q_{3/2}|\hat{S}^{+}_i|0\rangle\,|^2} \tag{5.19}$$

Similar derivation follows for $\hat{S}^{-}_i$. The corresponding expressions become

$$\langle \tilde{f}|H^{-}_{HF}|i\rangle = \frac{A}{\sqrt{N}}\sqrt{\sum_i \frac{1-P_i}{2}|\langle 0\rangle\,|\hat{S}^{-}_i|Q_{3/2}|^2} \tag{5.20}$$

and for $\hat{S}^{z}_i$ there will be an effective field with energy contribution

$$H^{z}_{HF} = A\sum_i P_i\hat{S}^{z}_i \tag{5.21}$$

The form of $|0\rangle$ also enters into the transitions. Let us focus on the (1,1,1) part

$$|0\rangle \simeq \alpha(\epsilon)\,|\uparrow\uparrow\downarrow\rangle + \beta(\epsilon)\,|\uparrow\downarrow\uparrow\rangle + \gamma(\epsilon)\,|\downarrow\uparrow\uparrow\rangle \tag{5.22}$$

The coefficients will depend on ϵ. More specifically in terms of the HI they will depend on the crossing between $|Q_{3/2}\rangle$ and $|0\rangle$ which happens at $\epsilon = \epsilon_c$. As the polarisation is changed this crossing will also change $\epsilon_c = \epsilon_c(P)$. The coefficients enter into the coupling through

$$\begin{aligned}\alpha_0 &= \langle Q_{3/2}|S_3^+|0\rangle = \langle 0|S_3^-|Q_{3/2}\rangle^* \\ \beta_0 &= \langle Q_{3/2}|S_2^+|0\rangle = \langle 0|S_2^-|Q_{3/2}\rangle^* \\ \gamma_0 &= \langle Q_{3/2}|S_1^+|0\rangle = \langle 0|S_1^-|Q_{3/2}\rangle^*\end{aligned} \tag{5.23}$$

where $\alpha_0 = \alpha(\epsilon_c)$ and so on.

Completing the expression for the coupling between them and inserting it into the Landau-Zener expression we get the transition probability

$$\begin{aligned}P_{LZ} &= 1 - \exp\left[-2\pi\frac{q_\pm^2}{\hbar v}\right] \\ q_\pm^2 &= \frac{A^2}{N}\left(\frac{1\pm P_1}{2}|\gamma_0|^2 + \frac{1\pm P_2}{2}|\beta_0|^2 + \frac{1\pm P_3}{2}|\alpha_0|^2\right) \\ v &= \frac{\partial E}{\partial \epsilon}\frac{\partial \epsilon}{\partial t}\end{aligned} \tag{5.24}$$

where the $\pm$ refers to which electron spin-flip is occurring. The coefficients can also be included into Eq.(5.19) to give

$$\begin{aligned}p_1 &= \frac{(1\pm P_1)|\gamma_0|^2}{(1\pm P_1)|\gamma_0|^2 + (1\pm P_2)|\beta_0|^2 + (1\pm P_3)|\alpha_0|^2} \\ p_2 &= \frac{(1\pm P_2)|\beta_0|^2}{(1\pm P_1)|\gamma_0|^2 + (1\pm P_2)|\beta_0|^2 + (1\pm P_3)|\alpha_0|^2} \\ p_3 &= \frac{(1\pm P_3)|\alpha_0|^2}{(1\pm P_1)|\gamma_0|^2 + (1\pm P_2)|\beta_0|^2 + (1\pm P_3)|\alpha_0|^2}\end{aligned} \tag{5.25}$$

for a given spin-flip happening in one of the dots. $\sum_i p_i = 1$ as it should be.

These forced and controlled spin-flips will compete against the natural relaxation of the nuclear spin polarisation. Let us make a short summary of this relaxation next.

5.2.1 Nuclear spin relaxation

The nuclear Zeeman-splitting is a very small energy splitting and will behave randomly even for small temperatures. This random behaviour will cause spin-flips of the nuclear spins and can be qualitatively investigated defining two spin-flip frequencies

$$\begin{aligned}\gamma_+ &= \mathcal{A}N^- = \mathcal{A}N\frac{1-P}{2} \\ \gamma_- &= \mathcal{A}N^+ = \mathcal{A}N\frac{1+P}{2}\end{aligned} \tag{5.26}$$

where $\mathcal{A}$ is a parameter governing the efficiency of these spin-flip processes. $\gamma_\pm$ is the frequency of $\pm$ spin-flips.

Eq.(5.26) can be understood by noting that $N^\mp$ are the available nuclei for $\pm$ spin-flips. Consider then the overall effect on the polarisation by one spin-flip

$$\Delta P = P(N^+ \pm 1) - P(N^+) = \frac{(N^+ \pm 1) - (N^- \mp 1)}{N} - \frac{(N^+ - N^-)}{N} = \pm\frac{2}{N} \tag{5.27}$$

This means that the change in polarisation due to $\gamma_\pm$ can be expressed

$$\frac{dP}{dt} = \frac{2}{N}(\gamma_+ - \gamma_-) = -2\mathcal{A}P \tag{5.28}$$

The quantity $2\mathcal{A} = 1/\tau$ is knows as the relaxation constant and depends on the material. Solving this differential equation yields

$$P(t) = P_0 e^{-t/\tau} \tag{5.29}$$

Where P_0 is the initial polarisation. This shows that on average the polarisation will relax down to zero.

At $P = 0$ we have $N^+ = N^- = \frac{N}{2}$ which means that on average $\gamma_+ = \gamma_-$. However these processes are random and will still cause the polarisation fluctuate around zero, but if polarisation starts to build up the relaxation will begin to force it back towards zero. The relaxation constant $\tau \sim 10$s for GaAs [40].

5.3 Numerical simulations

In this section we will consider the effect Landau-Zener transitions on the TQD have on the polarisation of nuclei on each dot. The general approach will be described as well as the result for specific sweeping procedures. The simulations was performed in Python using the packages scipy, pyplot, time and random. The code is added in the appendix.

5.3.1 Algorithm

In the numerical approach the system is initialised with different system parameters. Some of these, such as Δ, t, will be the same for all numerical procedures and determine the energies of the $S_z = \frac{1}{2}$ sub-space. Others can be varied to affect the probability of transitions such as initial polarisation P, external magnetic field B and the sweep speed $\frac{\partial\epsilon}{\partial\tau}$.

The effect of sweeping through a crossing will be different in the left crossing and the right crossing, Fig.5.7 a). The effective field will determine where the crossing happens, ϵ_c, which in turn will determine what the coefficients are for the $|0\rangle$ state

$$|0\rangle = \alpha(\epsilon)\,|\uparrow\uparrow\downarrow\rangle + \beta(\epsilon)\,|\uparrow\downarrow\uparrow\rangle + \gamma(\epsilon)\,|\downarrow\uparrow\uparrow\rangle \tag{5.30}$$

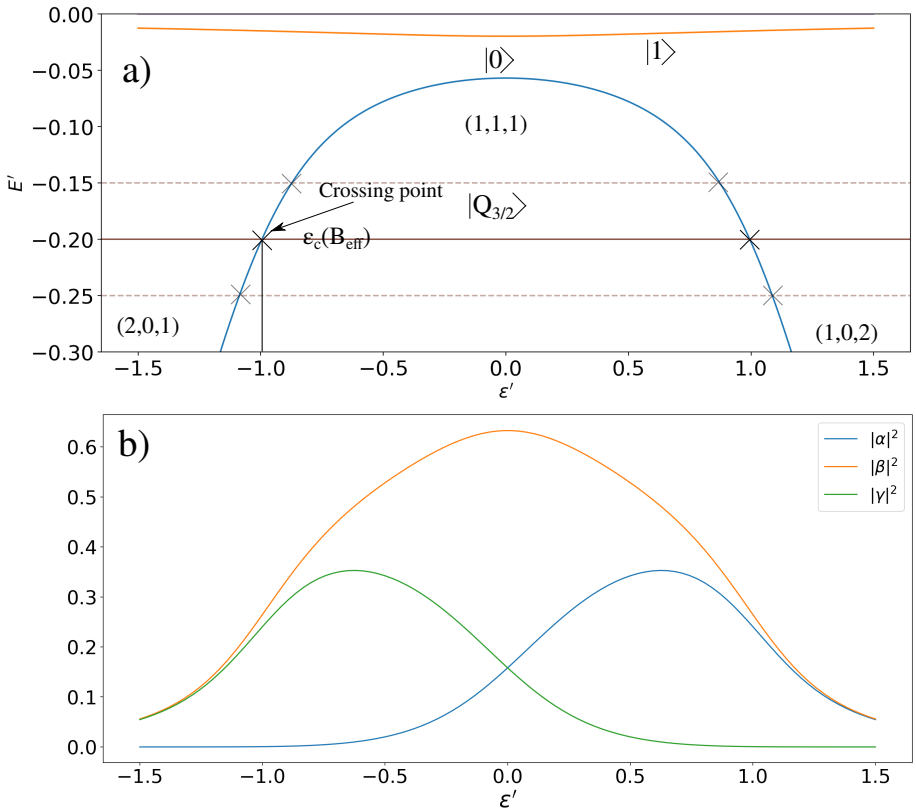

Figure 5.7: a) Energies of the system and crossing points $\epsilon = \epsilon_c$. Dashed lines illustrate the change of ϵ_c as the field varies. b) squared coefficients of the $|0\rangle$ state in basis $|\uparrow\uparrow\downarrow\rangle, |\uparrow\downarrow\uparrow\rangle, |\downarrow\uparrow\uparrow\rangle$. $\epsilon' = \frac{\epsilon}{\Delta}$ and $E' = \frac{E}{\Delta}$. $t = 0.2\Delta$ was used to enhance the splitting between $|0\rangle$ and $|1\rangle$

By going through the right crossing this will affect dot 1 and 2. While the left crossing will affect dot 2 and 3. This can be seen from the values of the coefficients at the crossing, Fig.5.7 b). Further we see that in the doubly occupied areas the coefficients are small as expected, and if the energy crossing happens here the probability of transition would be small.

Once a LZ-transition happens the polarisation, and as a consequence the effective field, changes. This leads to change in the system energies and change of the crossing points. Since some of the parameters of the system is changed so is the Hamiltonian, and it will need be solved again for each change of the system parameters. This leads to a routine illustrated in Fig.5.8. The Hamiltonian is solved to obtain the energy spectrum and the coefficients. A sweep through one of the crossings is performed with the possibility of a LZ-transition in one of the dots. This sweep will require some interval of time, and as this time goes

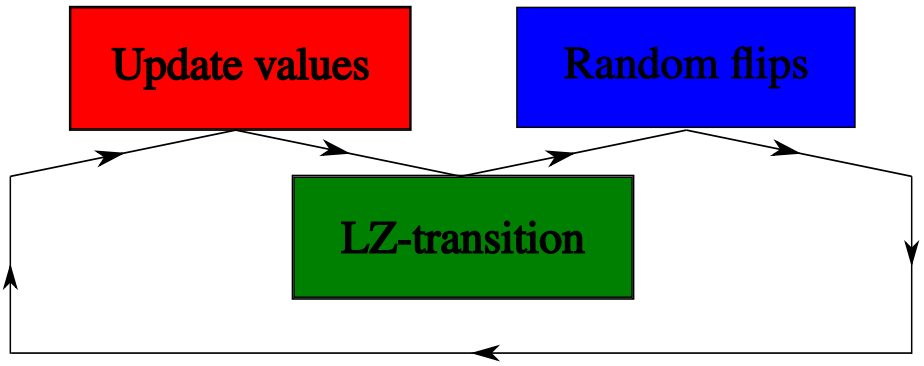

Figure 5.8: Order of the algorithm. The Hamiltonian is solved for the system parameters. Second comes a calculation to determine if a Landau-Zener transition (LZ) occurs and update of values accordingly. After LZ it checks for the effect of random spin-flips and updates values accordingly. These three steps are then repeated.

there is a chance that the nuclei will perform random spin-flips. If any changes occur the system parameters are updated. This cycle is then continued for the necessary number of sweeps n while looking at the evolution of the polarisation.

The random flips mentioned are the random fluctuations of the nuclear spin bath with typical value of the effective field $\frac{A}{\sqrt{N}}$[39]. The goal is for this procedure to reduce these random effects and therefore increase the coherence time of the system. The random flips have a characteristic relaxation time τ_{r}. The number of random flips happening during a sweep will depend on the ratio $\frac{\tau_{\mathrm{sweep}}}{\tau_{\mathrm{r}}}$, implying that the sweeps must happen with a sufficiently high frequency to outperform the random flips. In the algorithm the amount of random flips are determined by a Poisson distribution with expected value depending on the ratio between relaxation and sweep time and the system polarisation.

5.3.2 Results and discussion

Here we present the results from the different sweep procedures. We must stress that the values chosen are not necessarily physical, but chosen to elicit the overall effect of each procedure. All plots share the common parameters: $\Delta = 1$, $t = 0.1\Delta$, $A = \Delta$, $\frac{t_{sweep}}{\tau_{\mathrm{r}}} = 10^{-5}$ and $P_{\mathrm{init}} = [0.00, 0.00, 0.00]$. The remaining parameters are varied slightly: Initial Zeeman-energy E_{0Z}, sweeping speed $v_0 = \hbar\frac{\partial\epsilon}{\partial t}$, number of nuclei on the dot N. The number of sweeps was of order $n \sim 10^6$, sufficiently large to see any tendencies of the method.

We will be comparing the root-mean-square (RMS) values of the fluctuations over each dot, both for only random flips and for random flips with Landau-Zener transitions, denoted RMS^i and $\mathrm{RMS}^i_{\mathrm{LZ}}$ respectively with i indicating which dot. The goal is for Landau-Zener transitions to reduce the

magnitude of the fluctuations.

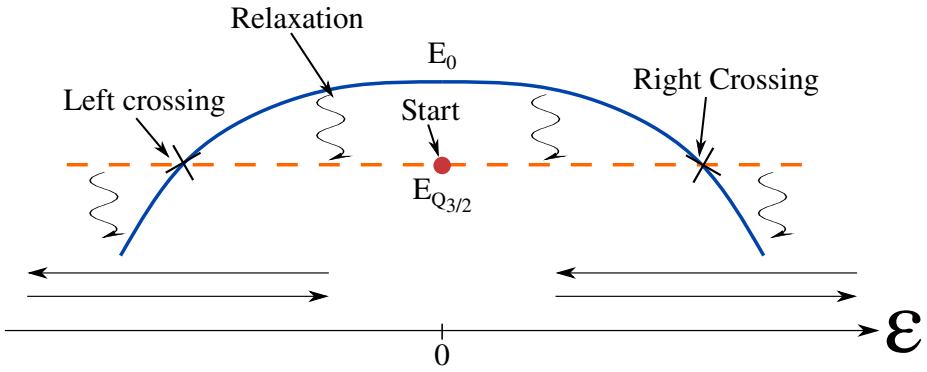

Figure 5.9: Begin at $\epsilon = 0$ in the $|Q_{3/2}\rangle$ state. Relaxation into ground state after each crossing.

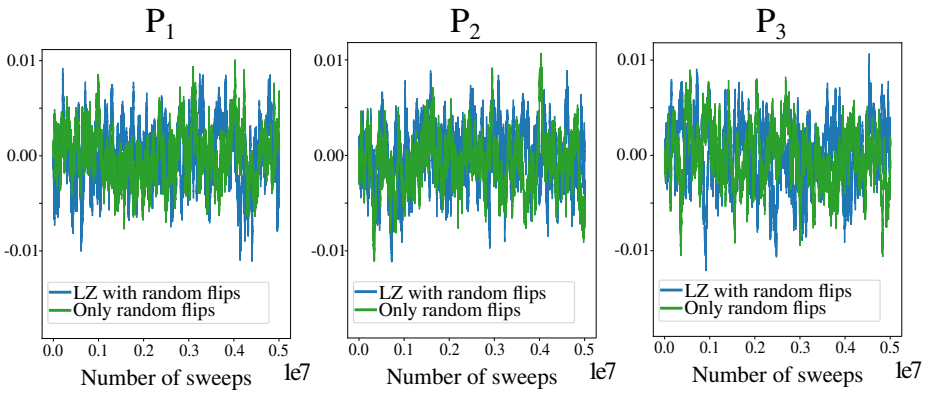

Figure 5.10: $N = 10^5$, $E_{0Z} = 0.15\Delta$, $v_0 = 10^{-6}\Delta^2$. RMS values: $\text{RMS}^1_{\text{LZ}} = 0.003$, $\text{RMS}^1 = 0.003$, $\text{RMS}^2_{\text{LZ}} = 0.003$, $\text{RMS}^2 = 0.003$, $\text{RMS}^3_{\text{LZ}} = 0.003$, $\text{RMS}^3 = 0.003$.

From the results we can see that mainly two procedures looks interesting to explore further, namely Fig.5.11 and Fig.5.15. The change in RMS value is not dramatic, but they are improved. Fig.5.11 seems to reduce the magnitude of fluctuations for each dot, which is in the end necessary to increase the coherence time of the system.

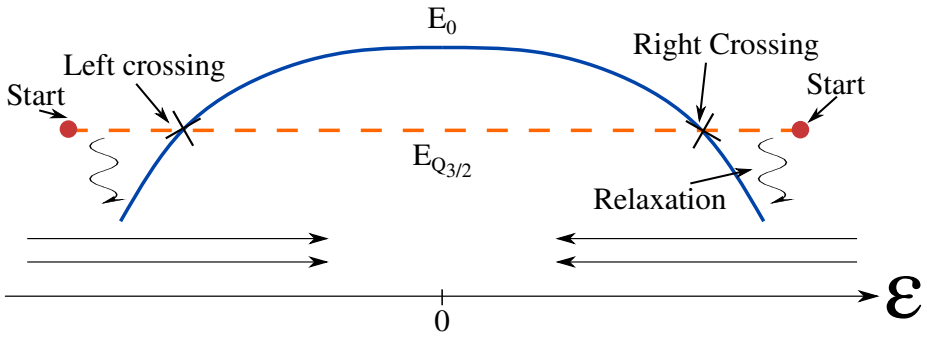

Figure 5.11: Begin at $|\epsilon| > \Delta$ in the $|0\rangle$ state. Go through the crossing. Alternate between beginning at left and right side.

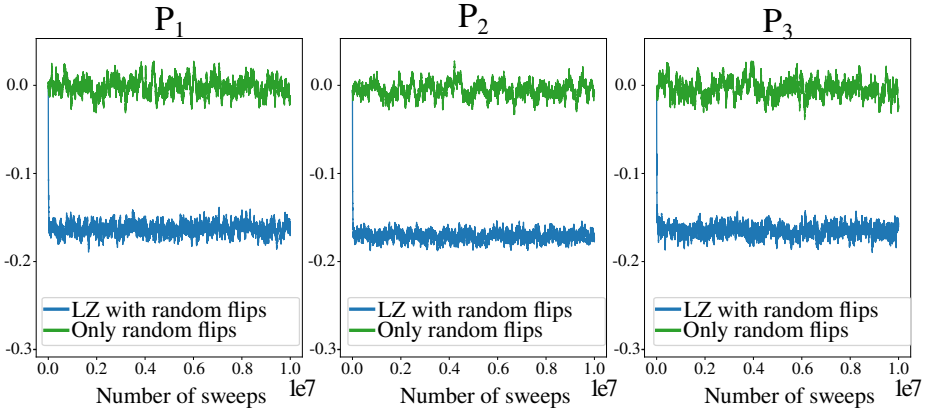

Figure 5.12: $N = 10^4$, $E_{0Z} = 0.025\Delta$, $v_0 = 10^{-5}\Delta^2$. RMS values: $\mathrm{RMS}^1_{\mathrm{LZ}} = 0.007$, $\mathrm{RMS}^1 = 0.009$, $\mathrm{RMS}^2_{\mathrm{LZ}} = 0.007$, $\mathrm{RMS}^2 = 0.010$, $\mathrm{RMS}^3_{\mathrm{LZ}} = 0.007$, $\mathrm{RMS}^3 = 0.010$.

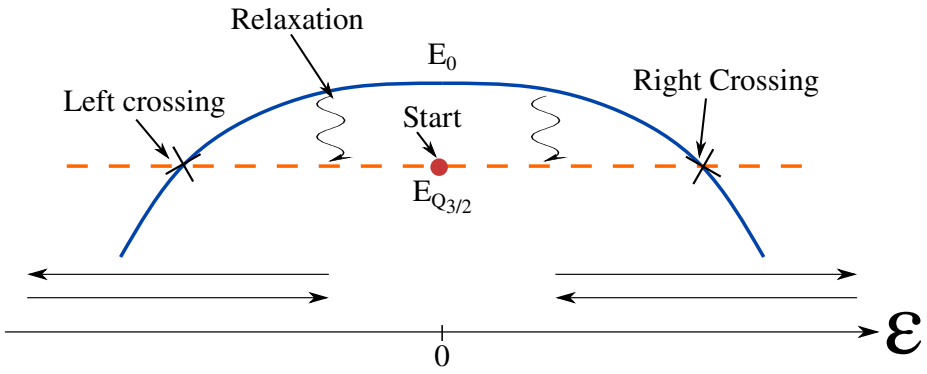

Figure 5.13: Begin at $\epsilon = 0$ in the $|Q_{3/2}\rangle$ state. Relaxation into ground state only in the regime $|\epsilon| < \Delta$.

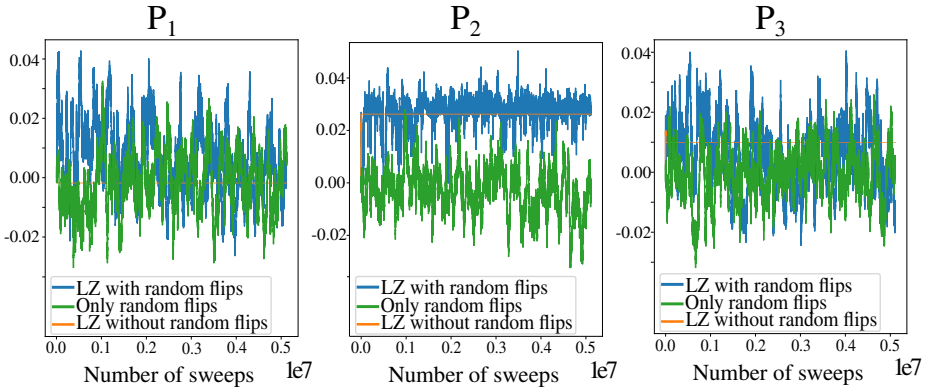

Figure 5.14: Here the pure Landau-Zener transition is also added to emphasise the 'pushing' it exerts towards the random flips. $N = 10^4$, $E_{0Z} = 0.025\Delta$, $v_0 = 10^{-5}\Delta^2$. RMS values: $\mathrm{RMS}^1_{\mathrm{LZ}} = 0.012$, $\mathrm{RMS}^1 = 0.001$, $\mathrm{RMS}^2_{\mathrm{LZ}} = 0.006$, $\mathrm{RMS}^2 = 0.009$, $\mathrm{RMS}^3_{\mathrm{LZ}} = 0.011$, $\mathrm{RMS}^3 = 0.009$.

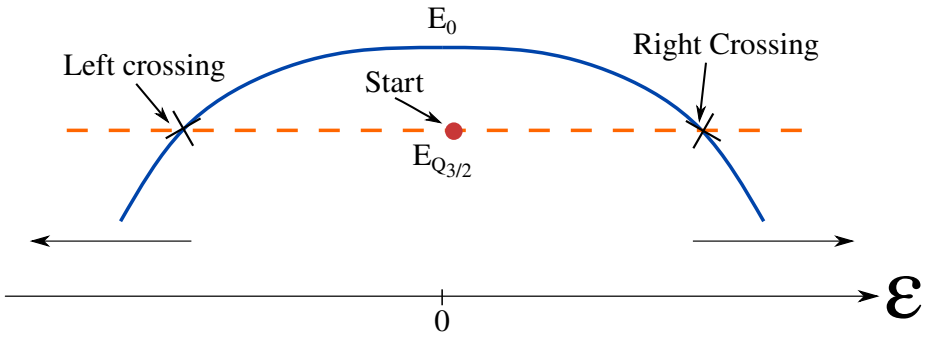

Figure 5.15: Begin at $\epsilon < -\Delta$ in the $|Q_{3/2}\rangle$ state. Sweep through the crossings without any relaxation.

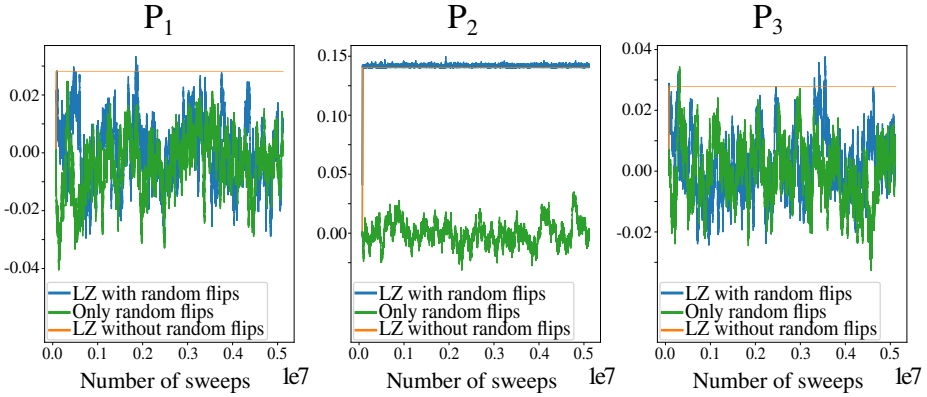

Figure 5.16: Here the pure Landau-Zener transition is also added to emphasise the 'pushing' it exerts towards the random flips. $N = 10^4$, $E_{0Z} = 0.1\Delta$, $v_0 = 10^{-5}\Delta^2$. RMS values: $\mathrm{RMS}^1_{\mathrm{LZ}} = 0.011$, $\mathrm{RMS}^1 = 0.010$, $\mathrm{RMS}^2_{\mathrm{LZ}} = 0.003$, $\mathrm{RMS}^2 = 0.010$, $\mathrm{RMS}^3_{\mathrm{LZ}} = 0.010$, $\mathrm{RMS}^3 = 0.010$.

5.4 Analytic approximation

In order to better understand the coupled electron-nuclear spin dynamics resulting from the different sweep procedures investigated above, we would like to develop an analytic framework to describe the time-dependence of the polarisations in the three dots. The first step will be made using perturbation theory.

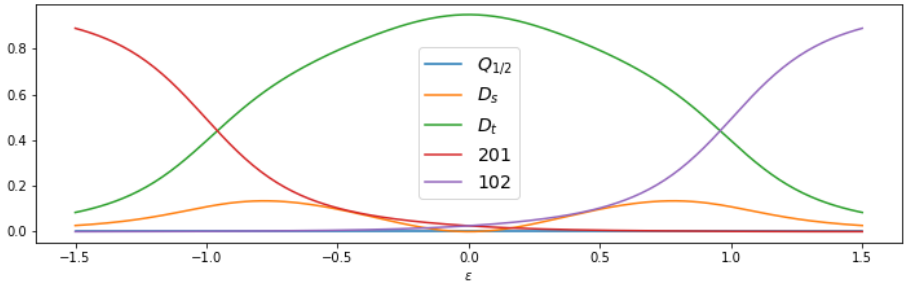

Figure 5.17: Squared coefficients of the $|0\rangle$ state found by numerical solution of the Hamiltonian (5.32). $\epsilon = \frac{\epsilon}{\Delta}$. $t = 0.2\Delta$

5.4.1 Perturbation theory for logical states

We will consider the basis

$$\begin{aligned} |D_T\rangle &= \frac{1}{\sqrt{6}}(|\uparrow\uparrow\downarrow\rangle - 2\,|\uparrow\downarrow\uparrow\rangle + |\downarrow\uparrow\uparrow\rangle) \\ |D_S\rangle &= \frac{1}{\sqrt{2}}(|\uparrow\uparrow\downarrow\rangle - |\downarrow\uparrow\uparrow\rangle) \\ |\uparrow 0S\rangle,&\ |S0\uparrow\rangle \end{aligned} \tag{5.31}$$

in which the Hamiltonian can be written as a four dimensional matrix

$$H = \begin{pmatrix} 0 & 0 & \frac{t}{2} & \frac{t}{2} \\ 0 & 0 & \frac{\sqrt{3}t}{2} & -\frac{\sqrt{3}t}{2} \\ \frac{t}{2} & \frac{\sqrt{3}t}{2} & \Delta_+ & 0 \\ \frac{t}{2} & -\frac{\sqrt{3}t}{2} & 0 & \Delta_- \end{pmatrix} \tag{5.32}$$

with $\Delta_\pm = \Delta \pm \epsilon$. Here both the Zeeman-energy and the Coulomb energy of the (1,1,1) configuration is shifted out. Any contribution from the nuclear gradient fields are also omitted for now.

Eigenstates of the Hamiltonian (5.32) is not straightforward to find through a process of diagonalisation. Therefore it is needed with some approximations. Looking at Fig.5.17 it is clear that $|S0\uparrow\rangle$ only have a small contribution for $\epsilon > 0$ and $|\uparrow 0S\rangle$ only have a small contribution for $\epsilon < 0$. So for each regime of ϵ the coupling to one of the doubly occupied states might be considered a perturbation, and will hopefully to a good approximation recreate the energy spectrum found numerically.

Let us consider the regime $\epsilon < 0$ and consider the coupling to $|\uparrow 0S\rangle$ as a

perturbation. The Hamiltonian can then be expressed

$$H = H_0 + V' = \begin{pmatrix} 0 & 0 & \frac{t}{2} & 0 \\ 0 & 0 & -\frac{\sqrt{3}t}{2} & 0 \\ \frac{t}{2} & -\frac{\sqrt{3}t}{2} & \Delta'_+ & 0 \\ 0 & 0 & 0 & \Delta'_- \end{pmatrix} + \begin{pmatrix} 0 & 0 & 0 & \frac{t}{2} \\ 0 & 0 & 0 & \frac{\sqrt{3}t}{2} \\ 0 & 0 & 0 & 0 \\ \frac{t}{2} & \frac{\sqrt{3}t}{2} & 0 & 0 \end{pmatrix} \tag{5.33}$$

The H_0 part can be diagonalised, which is clear by doing a change of basis

$$\begin{aligned} |\alpha\rangle &= \frac{1}{2}(\sqrt{3}\,|D_S\rangle + |D_T\rangle) \\ |\beta\rangle &= \frac{1}{2}(|D_S\rangle - \sqrt{3}\,|D_T\rangle) \end{aligned} \tag{5.34}$$

This leads to

$$H_0 = \begin{pmatrix} 0 & 0 & 0 & 0 \\ 0 & 0 & t & 0 \\ 0 & t & \Delta_+ & 0 \\ 0 & 0 & 0 & \Delta_- \end{pmatrix} \tag{5.35}$$

with eigenstates and eigenenergies

$$\begin{aligned} E_\pm &= \frac{\Delta_+}{2} \pm \sqrt{\left(\frac{\Delta_+}{2}\right)^2 + t^2} \\ |E_+\rangle &= \cos\frac{\theta}{2}\,|\beta\rangle + \sin\frac{\theta}{2}\,|S0\uparrow\rangle \\ |E_-\rangle &= \sin\frac{\theta}{2}\,|\beta\rangle - \cos\frac{\theta}{2}\,|S0\uparrow\rangle \\ \tan\theta &= \frac{2t}{\Delta_+} \end{aligned} \tag{5.36}$$

In the basis $\{|\alpha\rangle, |E_-\rangle, |E_+\rangle, |\uparrow 0S\rangle\}$ the Hamiltonian becomes

$$H = H_0 + V' = \begin{pmatrix} 0 & 0 & 0 & 0 \\ 0 & E_- & 0 & 0 \\ 0 & 0 & E_+ & 0 \\ 0 & 0 & 0 & \Delta'_- \end{pmatrix} + \begin{pmatrix} 0 & 0 & 0 & t_\alpha \\ 0 & 0 & 0 & t_- \\ 0 & 0 & 0 & t_+ \\ t_\alpha & t_- & t_+ & 0 \end{pmatrix} \tag{5.37}$$

with $t_\alpha = \frac{\sqrt{3}t}{2}$, $t_+ = -\frac{t}{2}\cos\frac{\theta}{2}$, $t_- = -\frac{t}{2}\sin\frac{\theta}{2}$. Since we are using the crossing between $|0\rangle$ and $|Q_{3/2}\rangle$ for our Landau-Zener transitions it is here only necessary to find an expression for this $|0\rangle$ state.

The state with lowest energy is $|E_-\rangle$ so we only need the effect of the perturbation on this state. Additionally let us assume that $\min(\Delta E_{-+}) = \min(E_+ - E_-) = 2t$ is much larger than the perturbation, such that these states are always sufficiently far apart. Then it is enough to consider only how $|\alpha\rangle$ and $|E_-\rangle$ is affected by V'.

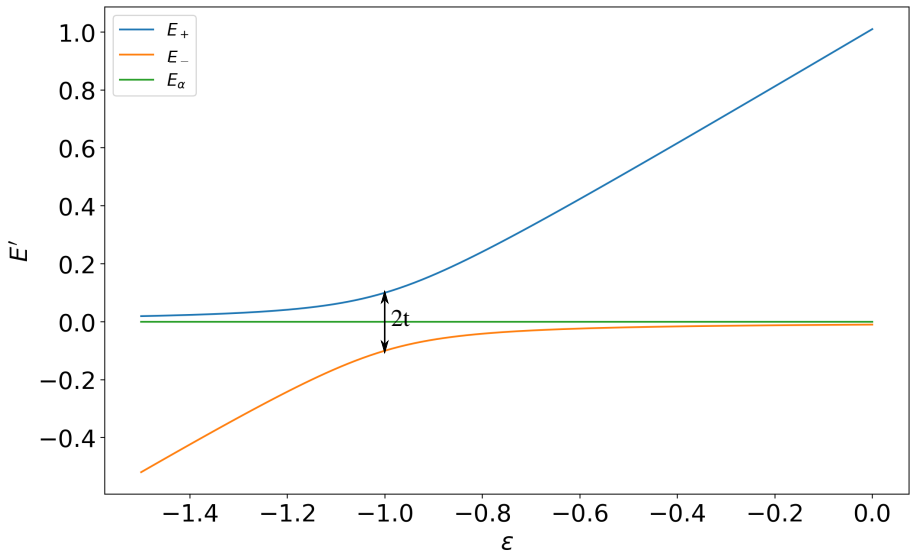

Figure 5.18: The energy spectrum of H_0. The energies Δ'_- corresponding to $|\uparrow 0S\rangle$ will be higher up from these again. $\epsilon' = \frac{\epsilon}{\Delta}$, $E' = \frac{E'}{\Delta}$.

Limiting ourselves to the subsystem $\{|\alpha\rangle, |E_-\rangle\}$ and looking at the effect of the perturbation using Schrieffer-Wolff transformation Eq.(4.7), the effective Hamiltonian becomes

$$\begin{aligned} H &= \begin{pmatrix} -\frac{t_\alpha^2}{\Delta_-} & \frac{1}{2}t_\alpha t_- \left(-\frac{1}{\Delta_-} + \frac{1}{E_- - \Delta_-}\right) \\ \frac{1}{2}t_\alpha t_- \left(-\frac{1}{\Delta_-} + \frac{1}{E_- - \Delta_-}\right) & E_- + \frac{t_-^2}{E_- - \Delta_-} \end{pmatrix} \\ &= \begin{pmatrix} E_a & t_{ab} \\ t_{ab} & E_b \end{pmatrix} \end{aligned} \tag{5.38}$$

The corresponding $|0\rangle$ state will then be on the form

$$\begin{aligned} E_0 &= \frac{E_a + E_b}{2} - \sqrt{\left(\frac{E_a - E_b}{2}\right)^2 + t_{ab}^2} \\ |0\rangle &= \sin\frac{\theta'}{2}|\alpha\rangle - \cos\frac{\theta'}{2}|E_-\rangle \\ \tan\theta' &= \frac{2t_{ab}}{(E_a - E_b)} \end{aligned} \tag{5.39}$$

where the perturbation of the $|\alpha\rangle, |E_-\rangle$ states are considered negligible. This is then the approximated expressions for $|0\rangle$ state and its energy.

We can write out the expression for $|0\rangle$ to get the coefficients

$$\begin{aligned}
|0\rangle &\simeq \sin\frac{\theta'}{2}\,|\alpha\rangle - \cos\frac{\theta'}{2}\,|E_-\rangle \\
&= \sin\frac{\theta'}{2}\left(\frac{1}{2}(\sqrt{3}\,|D_S\rangle + |D_T\rangle)\right) - \cos\frac{\theta'}{2}\sin\frac{\theta}{2}\left(\frac{1}{2}(|D_S\rangle - \sqrt{3}\,|D_T\rangle\right) \\
&= \frac{1}{2}\left(\sqrt{3}\sin\frac{\theta'}{2} - \cos\frac{\theta'}{2}\sin\frac{\theta}{2}\right)|D_S\rangle + \frac{1}{2}\left(\sin\frac{\theta'}{2} + \sqrt{3}\cos\frac{\theta'}{2}\sin\frac{\theta}{2}\right)|D_T\rangle \\
&= \sqrt{\frac{2}{3}}\sin\frac{\theta'}{2}\,|\uparrow\uparrow\downarrow\rangle - \sqrt{\frac{1}{6}}\left(\sin\frac{\theta'}{2} + \sqrt{3}\cos\frac{\theta'}{2}\sin\frac{\theta}{2}\right)|\uparrow\downarrow\uparrow\rangle - \\
&\quad \sqrt{\frac{1}{6}}\left(\sin\frac{\theta'}{2} - \sqrt{3}\cos\frac{\theta'}{2}\sin\frac{\theta}{2}\right)|\downarrow\uparrow\uparrow\rangle
\end{aligned} \tag{5.40}$$

from where we can identify $\{\alpha, \beta, \gamma\}$.

Let us now consider the regime $\epsilon > 0$. All the same approximations will be assumed with $|S0\uparrow\rangle$ and $|\uparrow 0S\rangle$ switching roles. Begin again with the Hamiltonian (5.32) and consider the $|S0\uparrow\rangle$ as a perturbation

$$H = H_0 + V' = \begin{pmatrix} 0 & 0 & \frac{t}{2} & 0 \\ 0 & 0 & \frac{\sqrt{3}t}{2} & 0 \\ \frac{t}{2} & \frac{\sqrt{3}t}{2} & \Delta_- & 0 \\ 0 & 0 & 0 & \Delta_+ \end{pmatrix} + \begin{pmatrix} 0 & 0 & 0 & \frac{t}{2} \\ 0 & 0 & 0 & -\frac{\sqrt{3}t}{2} \\ 0 & 0 & 0 & 0 \\ \frac{t}{2} & -\frac{\sqrt{3}t}{2} & 0 & 0 \end{pmatrix} \tag{5.41}$$

Do a similar change of basis

$$\begin{aligned}
|\gamma\rangle &= \frac{1}{2}(\sqrt{3}\,|D_S\rangle - |D_T\rangle) \\
|\delta\rangle &= \frac{1}{2}(|D_S\rangle + \sqrt{3}\,|D_T\rangle)
\end{aligned} \tag{5.42}$$

which in the basis $\{|\gamma\rangle, |E_-\rangle, |E_+\rangle, |\uparrow 0S\rangle\}$ results in

$$H = H_0 + V' = \begin{pmatrix} 0 & 0 & 0 & 0 \\ 0 & E_- & 0 & 0 \\ 0 & 0 & E_+ & 0 \\ 0 & 0 & 0 & \Delta_+ \end{pmatrix} + \begin{pmatrix} 0 & 0 & 0 & t_\gamma \\ 0 & 0 & 0 & t_- \\ 0 & 0 & 0 & t_+ \\ t_\gamma & t_- & t_+ & 0 \end{pmatrix} \tag{5.43}$$

where

$$
\begin{aligned}
E_{\pm} &= \frac{\Delta_-}{2} \pm \sqrt{\left(\frac{\Delta_-}{2}\right)^2 + t^2} \\
|E_+\rangle &= \cos\frac{\theta}{2}\,|\delta\rangle + \sin\frac{\theta}{2}\,|\uparrow 0S\rangle \\
|E_-\rangle &= \sin\frac{\theta}{2}\,|\delta\rangle - \cos\frac{\theta}{2}\,|\uparrow 0S\rangle \\
\tan\theta &= \frac{2t}{\Delta_-}
\end{aligned}
\tag{5.44}
$$

with $t_\gamma = \frac{\sqrt{3}t}{2}$, $t_+ = -\frac{t}{2}\cos\frac{\theta}{2}$, $t_- = -\frac{t}{2}\sin\frac{\theta}{2}$. We are still only interested in the approximated $|0\rangle$ state, so we therefore focus on the $|E_-\rangle, |\gamma\rangle$ part of the Hamiltonian.

$$
\begin{aligned}
H &= \begin{pmatrix} -\frac{t_\gamma^2}{\Delta_+} & \frac{1}{2}t_\gamma t_- \left(-\frac{1}{\Delta_+} + \frac{1}{E_- - \Delta_+}\right) \\ \frac{1}{2}t_\gamma t_- \left(-\frac{1}{\Delta_+} + \frac{1}{E_- - \Delta_+}\right) & E_- + \frac{t_-^2}{E_- - \Delta_+} \end{pmatrix} \\
&= \begin{pmatrix} E_c & t_{cd} \\ t_{cd} & E_d \end{pmatrix}
\end{aligned}
\tag{5.45}
$$

The corresponding $|0\rangle$ state will then be on the form

$$
\begin{aligned}
E_0 &= \frac{E_c + E_d}{2} - \sqrt{\left(\frac{E_c - E_d}{2}\right)^2 + t_{cd}^2} \\
|0\rangle &= \sin\frac{\theta}{2}\,|\gamma\rangle - \cos\frac{\theta}{2}\,|E_-\rangle \\
\tan\theta &= \frac{2t_{cd}}{(E_c - E_d)}
\end{aligned}
\tag{5.46}
$$

Let us again write out the expression for $|0\rangle$ to get the coefficients

$$
\begin{aligned}
|0\rangle &\simeq \sin\frac{\theta'}{2}\,|\gamma\rangle - \cos\frac{\theta'}{2}\,|E_-\rangle \\
&= \sin\frac{\theta'}{2}\left(\frac{1}{2}(\sqrt{3}\,|D_S\rangle - |D_T\rangle)\right) - \cos\frac{\theta'}{2}\sin\frac{\theta}{2}\left(\frac{1}{2}(|D_S\rangle + \sqrt{3}\,|D_T\rangle\right) \\
&= \frac{1}{2}\left(\sqrt{3}\sin\frac{\theta'}{2} - \cos\frac{\theta'}{2}\sin\frac{\theta}{2}\right)|D_S\rangle - \frac{1}{2}\left(\sin\frac{\theta'}{2} + \sqrt{3}\cos\frac{\theta'}{2}\sin\frac{\theta}{2}\right)|D_T\rangle \\
&= \sqrt{\frac{1}{6}}\left(\sin\frac{\theta'}{2} - \sqrt{3}\cos\frac{\theta'}{2}\sin\frac{\theta}{2}\right)|\uparrow\uparrow\downarrow\rangle + \\
&\quad \sqrt{\frac{1}{6}}\left(\sin\frac{\theta'}{2} + \sqrt{3}\cos\frac{\theta'}{2}\sin\frac{\theta}{2}\right)|\uparrow\downarrow\uparrow\rangle - \sqrt{\frac{2}{3}}\sin\frac{\theta'}{2}\,|\downarrow\uparrow\uparrow\rangle
\end{aligned}
\tag{5.47}
$$

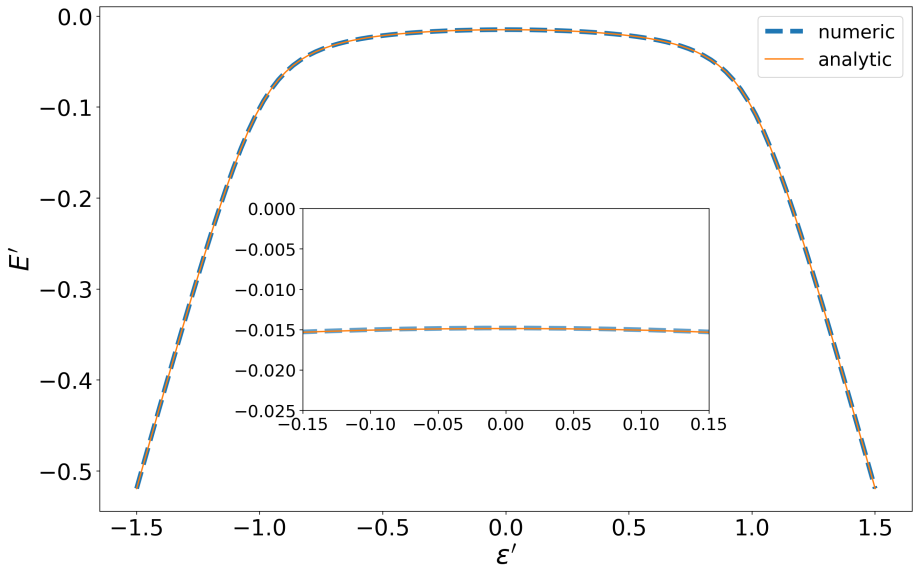

Figure 5.19: Comparison between analytic and numerical energies. $E' = \frac{E}{\Delta}$ and $\epsilon' = \frac{\epsilon}{\Delta}$. There is good accordance between numerical and analytic results even for $\epsilon \simeq 0$.

from where we can identify $\{\alpha, \beta, \gamma\}$ for $\epsilon > 0$.

Comparing the energy expressions Eq.(5.46) and Eq.(5.39) they are symmetric and can be put together into one expression by $\epsilon \to -|\epsilon|$ in Eq.(5.39) or $\epsilon \to |\epsilon|$ in Eq.(5.46). For the coefficients the following relation holds

$$\begin{aligned} \alpha_- &\leftrightarrow -\gamma_+ \\ \beta_- &\leftrightarrow -\beta_+ \\ \gamma_- &\leftrightarrow -\alpha_+ \end{aligned} \tag{5.48}$$

5.4.2 Results and discussion

To see the validity of the analytic expressions we compare them to the numerical exact solution. This is seen in Fig.5.19 and Fig.5.20. The analytic expressions closely resembles the numerical solution even for $\epsilon \simeq 0$ where it should be weakest. Thus in the absence of nuclear gradient fields the $|0\rangle$ state can be expressed in an analytic manner.

The next step in this direction is to include the effect of the nuclear field gradients and see how this affects the solution. This will show up as both addition to the energy and coupling between the states. The expressions found here have a symmetry about $\epsilon = 0$. This symmetry is in general expected to be broken when gradient fields are included.

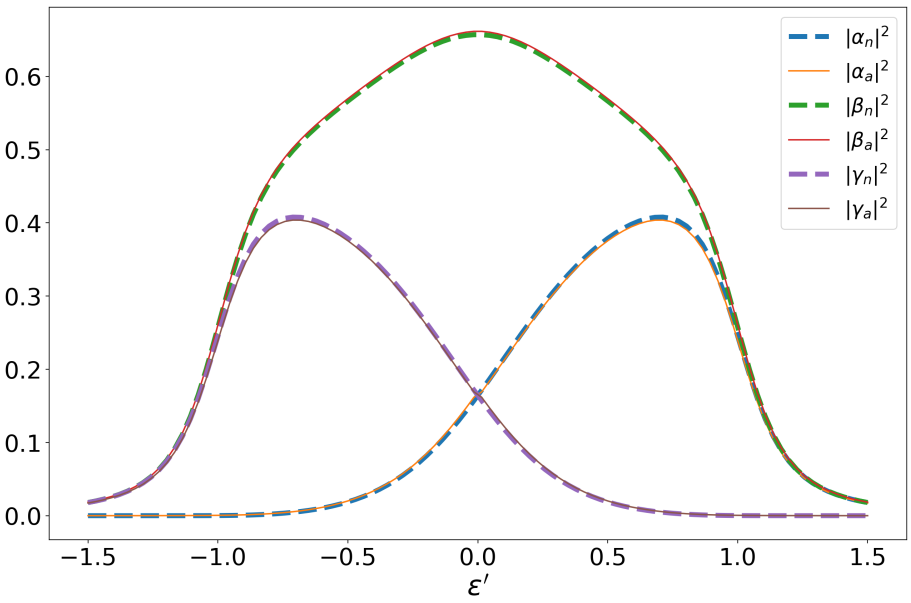

Figure 5.20: Comparison between analytic and numerical state coefficients squared. $E' = \frac{E}{\Delta}$ and $\epsilon' = \frac{\epsilon}{\Delta}$. There is good accordance between numerical and analytic results even for $\epsilon \simeq 0$.

Chapter 6

Conclusion

We have investigated how Landau-Zener transitions between $|Q_{3/2}\rangle$ and $|0\rangle$ in the TQD can affect the magnitude of fluctuations of the nuclear gradient fields. By using smart sweep procedures we were able to indeed reduce this magnitude, see Fig.5.12 and Fig.5.16. Simulations show that it is choice of procedure which determines if any suppression can be obtained, and parameters chosen will determine the strength of the suppression. The parameters used in this simulation where chosen to elicit the effect of the different procedures, and further analysis must be conducted in order to quantify this effect. The main question is how much such a procedure can increase the coherence time of the system.

Motivated by the result of the numerical simulation the first steps toward an analytic framework for the time dependence of the polarisation have also been made. By applying perturbation theory to the Hamiltonian and treating the regions of $\epsilon < 0$ and $\epsilon > 0$ we were able to produce an accurate solution for the $|0\rangle$ state when nuclear field gradients is neglected.

The next step forward is to incorporate the nuclear field gradients into the Hamiltonian expressed by the analytic expressions. If this can be done the eigenstates of the system can be to a good approximation given by analytic expressions, possibly taking another step towards a good understanding of the time dependence of the polarisation in the system during the Landau-Zener sweeps.

Appendix A

Code

```
import scipy as sc
import matplotlib.pyplot as plt
import scipy.linalg as LA
import random as rnd
import time
from scipy.stats import poisson

def isFlip(v, a, b, c):
    """
    Checks if a LZ transition happens and which dot it happens in

    v = sweep speed

    a,b,c = coupling coefficients from hyperfine interaction
    """
    Dot = sc.array([0,0,0])
    prob = 1   sc.exp( (2 * sc.pi) * (a**2 + b**2 + c**2) / (4 * v)
    )
#     print('a = {}, b = {}, c = {}, prob = {}'.format(a,b,c,prob))
    flip = False
    if (prob > rnd.random()):
        flip = True
        N1 = (a * a) / (a * a + b * b + c * c)
        N2 = (b * b) / (a * a + b * b + c * c)
        N3 = (c * c) / (a * a + b * b + c * c)
        r = rnd.random()
        dot = 0
        if (N1 >= r):
            Dot[2] = 1
        elif (N1 + N2 >= r):
            Dot[1] = 1
        else:
            Dot[0] = 1

    return Dot, flip

def customEigh(H,var,delta,AP):
```

```
    """
    Handle the sorting of two lowest crossing eigenstates
    of a Hamiltonian where one of the values is known. The
    eigenstates needs to be uncoupled.

    This also finds where the energies cross
    ----------------------------------------------------

    H is the Hamiltonian

    var is the variable

    AP is array of effective field over each dot
    ----------------------------------------------------
    """
    switch1 = False
    switch2 = False
    idx1 = 1
    idx2 = 1

    eigVal = sc.zeros((len(var),len(H)))
    eigVec1 = sc.zeros((len(var),len(H)))
    eigVec2 = sc.zeros((len(var),len(H)))

    for idx,value in enumerate(var):

        H[4, 4] = delta + value + AP[2]
        H[5, 5] = delta   value + AP[0]

        eigval,eigvec = LA.eigh(H)
        eigVal[idx,:] = eigval
        if(eigval[0] == H[0,0]):

            if(idx1 == 1 and idx2 == 1):
                idx1 = idx

            eigVal[idx,0] = eigval[1]
            eigVal[idx,1] = eigval[0]
            eigVec1[idx,:] = eigvec[:,1]
            eigVec2[idx,:] = eigvec[:,0]
        else:

            if(not idx1 == 1 and idx2 == 1):
                idx2 = idx

            eigVal[idx,0] = eigval[0]
            eigVal[idx,1] = eigval[1]
            eigVec1[idx,:] = eigvec[:,0]
            eigVec2[idx,:] = eigvec[:,1]

    return [eigVal,eigVec1,eigVec2,idx1,idx2]

def sweep(v0,idx,B,evec,eigval,var,string):
    """
    Generalized sweep procedure

    v0 = the constant velocity
```

```
    idx = index of crossing, input must correspond to right
    or left crossing
    B = coupling field, input must correspond to right or
    left crossing
    evec = eigenvector of groundstate from customEigh
    eigval = eigenvalues from customEigh
    var = variable iterated over
    string = which transition (E.g 'Q0' or '0Q')
    """
    if(idx == 1):
        a = b = c = 0
        v = 1
    else:
        a = evec[idx, 3] * B[2]
        b = evec[idx, 2] * B[1]
        c = evec[idx, 1] * B[0]
        v = v0 * abs((eigval[idx+1,0] eigval[idx 1,0])/(2*(var[idx
    ] var[idx 1])))

    Dot,flip = isFlip(v,a,b,c)
    if(string == '0Q'):
        Dot *= 1

    return Dot, flip

def sweepRoutine12(m,ts,bool1,bool2):
    """
    Left crossing with mid initialization

    m is number of sweeps

    bool1 determines if LZ transitions are included

    bool2 determines if random spin flips are included

    Sweep template:
     ------------------
    |                  |
    |   Update values  |   > if(change)
    |------------------|
     ------------------
    |                  |   > if(flip)
    |   LZ Transition  |   updates flip accordingly
    |------------------|
     ------------------
    |                  |
    |   Random flips   |   > change = True
    |------------------|

            *

            *

            *
    """
    res = 10**2  #resolution
    delta = 1  #100 200E 6 eV
```

```
150     t = 0.1 * delta #tunneling coupling
151     eps = sc.linspace( 1.5 * delta, 1.5 * delta, res) #tuning
        parameter
152
153     flip = True
154     change = False
155
156     n = m  #number of sweeps
157     N = 1E+5  #number of nuclei
158     dP = 2.0 / N  #change in polarization
159     E0z = 6*t**2/delta # corresponds to B0 ~ 370 mT
160     A = 1*delta  #coupling factor between nuclei and dot
161     v0 = 1E 5
162     tsweep = ts#1E 4 #factor for random spin flips based on sweep
        frequency
163
164     P1storage = sc.zeros(n) #returned array
165     P2storage = sc.zeros(n)
166     P3storage = sc.zeros(n)
167
168     Dot = sc.zeros(3)
169     P = sc.array([ .0 ,.0 , .0])#sc.array([ .01 ,.01 , .01])#inital
        spin polarization
170     Bp = [0.0, 0.0, 0.0]  #effective positive field
171     Bm = [0.0, 0.0, 0.0]  #effective negative field
172
173     H = sc.zeros((6, 6)) #initialize matrix
174     eigval = sc.zeros((res, 6)) #initialize eigenvalue
175     eigvec1 = sc.zeros((res, 6)) #initialize eigenvector for 0
        state
176     eigvec2 = sc.zeros((res, 6)) #initialize eigenvector for Q
        state (not used)
177
178     #Triple dot interaction
179     #Same for all sweeps
180     H[1, 5] = H[5, 1] = H[2, 4] = H[4, 2] = t / sc.sqrt(2)
181     H[2, 5] = H[5, 2] = H[3, 4] = H[4, 3] =  H[1, 5]
182
183     for i in range(n):  #loops for number of sweeps
184
185         P1storage[i] = P[0] #update i value
186         P2storage[i] = P[1]
187         P3storage[i] = P[2]
188
189         if((change or flip) and bool1):
190             change = False
191             #update fields
192             #
    ##################################################################

193             #Effective field positive electron flip
194             Bp = [A / sc.sqrt(N) * sc.sqrt(((1 + P[i]) / 2)) for i
    in range(3)]
195             #Effective field negative electron flip
196             Bm = [A / sc.sqrt(N) * sc.sqrt(((1   P[i]) / 2)) for i
    in range(3)]
197             #Updated Zeeman energy taking polarization into account
```

```
198             Ez =  (E0z    sum(A * P))
199             #
    ##################################################################


200
201             #update and (re )diagonalize the matrix
202             #
    ##################################################################

203             H[0, 0] = Ez
204             H[1, 1] =  A * P[0] + A * P[1] + A * P[2]
205             H[2, 2] = +A * P[0]   A * P[1] + A * P[2]
206             H[3, 3] = +A * P[0] + A * P[1]   A * P[2]
207
208             #calculate the eigenvalues and eigenvector
209             eigval,eigvec1,eigvec2,idx1,idx2 = customEigh(H,eps,
    delta,A*P)
210
211             #
    ##################################################################


212
213         ####################
214         ###First crossing###
215         ####################
216
217         #################
218         ### Left side ###
219         #################
220
221         #############
222         ###0   > Q###
223         #############
224         if(bool1):
225             Dot, flip = sweep(v0,idx1,Bp,eigvec1,eigval,eps,'0Q')
226             P += Dot*dP
227             #
    ##################################################################


228
229         #random flips
230         if(bool2):
231
232             Np = N/2*(1+P)
233             Nm = N/2*(1 P)
234
235             pFlip = sc.array([poisson.rvs(tsweep*Np[i],size=1)[0]
    for i in range(3)])
236             mFlip = sc.array([poisson.rvs(tsweep*Nm[i],size=1)[0]
    for i in range(3)])
237
238             P += dP*(mFlip   pFlip)
239             change = True
240
241         if((change or flip) and bool1):
242             change = False
243             #update fields
```

```
244             #
    ######################################################################

245             #Effective field positive electron flip
246             Bp = [A / sc.sqrt(N) * sc.sqrt(((1 + P[i]) / 2)) for i
    in range(3)]
247             #Effective field negative electron flip
248             Bm = [A / sc.sqrt(N) * sc.sqrt(((1   P[i]) / 2)) for i
    in range(3)]
249             #Updated Zeeman energy taking polarization into account
250             Ez =  (E0z   sum(A * P))
251             #
    ######################################################################


252
253             #update and (re )diagonalize the matrix
254             #
    ######################################################################

255             H[0, 0] = Ez
256             H[1, 1] =  A * P[0] + A * P[1] + A * P[2]
257             H[2, 2] = +A * P[0]   A * P[1] + A * P[2]
258             H[3, 3] = +A * P[0] + A * P[1]   A * P[2]
259
260             #calculate the eigenvalues and eigenvector
261             eigval,eigvec1,eigvec2,Index1,Index2 = customEigh(H,eps
    ,delta,A*P)
262             #
    ######################################################################


263
264         ##################
265         ###Right side ###
266         ##################
267
268         if(bool1):
269             ##############
270             ###Q   > 0###
271             ##############
272             Dot, flip = sweep(v0,idx1,Bm,eigvec1,eigval,eps,'Q0')
273             P += Dot*dP
274             #
    ######################################################################


275
276
277         #random flips
278         if(bool2):
279
280             Np = N/2*(1+P)
281             Nm = N/2*(1 P)
282
283             pFlip = sc.array([poisson.rvs(tsweep*Np[i],size=1)[0]
    for i in range(3)])
284             mFlip = sc.array([poisson.rvs(tsweep*Nm[i],size=1)[0]
    for i in range(3)])
285
```

```
286                 P += dP*(mFlip     pFlip)
287                 change = True
288 
289     return P1storage, P2storage, P3storage
```

Bibliography

[1] Joseph F. Mulligan. "Heinrich Hertz and the Development of Physics". In: *Phys. Today* 42.3 (1989), pp. 50–57. DOI: 10.1063/1.881211.

[2] A. B. Arons and M. B. Peppard. "Einstein's Proposal of the Photon Concept - a Translation of the Ann. Phys. (Berl.) Paper of 1905". In: *Am. J. Phys.* 33.5 (1965), pp. 367–374. DOI: 10.1119/1.1971542.

[3] Gilbert N. Lewis. "The Conservation of Photons". In: *Nature* 118.2981 (1926), pp. 874–875. ISSN: 1476-4687. DOI: 10.1038/118874a0.

[4] William A. Fedak and Jeffrey J. Prentis. "The 1925 Born and Jordan paper "On quantum mechanics"". In: *Am. J. Phys.* 77.2 (2009), pp. 128–139. DOI: 10.1119/1.3009634.

[5] E. Schrödinger. "Quantisierung als Eigenwertproblem". In: *Ann. Phys. (Berl.)* 384.4 (1926), pp. 361–376. DOI: 10.1002/andp.19263840404.

[6] P. A. M. Dirac. "The Quantum Theory of the Electron". In: *Proc. Royal Soc. A* 117.778 (1928), pp. 610–624. DOI: 10.1098/rspa.1928.0023.

[7] Richard P. Feynman. "Simulating physics with computers". In: *Int. J. Theor. Phys.* 21.6-7 (1982), pp. 467–488. DOI: 10.1007/bf02650179.

[8] P.W. Shor. "Algorithms for quantum computation: discrete logarithms and factoring". In: *Proceedings 35th Annual Symposium on Foundations of Computer Science*. IEEE Comput. Soc. Press., 1994, pp. 124–134. DOI: 10.1109/sfcs.1994.365700.

[9] Lieven M. K. Vandersypen et al. "Experimental realization of Shor's quantum factoring algorithm using nuclear magnetic resonance". In: *Nature* 414.6866 (2001), pp. 883–887. DOI: 10.1038/414883a.

[10] A. Politi, J. C. F. Matthews, and J. L. O'Brien. "Shor's Quantum Factoring Algorithm on a Photonic Chip". In: *Science* 325.5945 (2009), pp. 1221–1221. DOI: 10.1126/science.1173731.

[11] John Preskill. "Quantum computing and the entanglement frontier - Rapporteur talk at the 25th Solvay Conference". In: *arXiv:1203.5813 [quant-ph]* (2012).

[12] Edwin Pednault et al. “Breaking the 49-Qubit Barrier in the Simulation of Quantum Circuits”. In: *arXiv:1710.05867 [quant-ph]* (2017).

[13] David P. DiVincenzo. “The Physical Implementation of Quantum Computation”. In: *Fortschritte der Physik* 48.9-11 (2000), pp. 771–783. DOI: 10.1002/1521-3978(200009)48:9/11<771::aid-prop771>3.0.co;2-e.

[14] PJM Peter Peters. *Electrical transport properties of the two-dimensional electron gas on liquid helium in high magnetic fields*. en. 1994. DOI: 10.6100/ir423028.

[15] S Subramanian. “High electron mobility transistors”. In: *Bull. Mater. Sci.* 13.1-2 (1990), pp. 121–133. DOI: 10.1007/bf02744866.

[16] A.Y. Cho and J.R. Arthur. “Molecular beam epitaxy”. In: *Prog. Solid State Ch.* 10 (1975), pp. 157–191. DOI: 10.1016/0079-6786(75)90005-9.

[17] G Owen. “Electron lithography for the fabrication of microelectronic devices”. In: *Rep. Prog. Phys.* 48.6 (1985), pp. 795–851. DOI: 10.1088/0034-4885/48/6/002.

[18] L P Kouwenhoven, D G Austing, and S Tarucha. “Few-electron quantum dots”. In: *Rep. Prog. Phys.* 64.6 (2001), pp. 701–736. DOI: 10.1088/0034-4885/64/6/201.

[19] Daniel Loss and David P. DiVincenzo. “Quantum computation with quantum dots”. In: *Phys. Rev. A* 57.1 (1998), pp. 120–126. DOI: 10.1103/physreva.57.120.

[20] Adriano Barenco et al. “Elementary gates for quantum computation”. In: *Phys. Rev. A* 52.5 (1995), pp. 3457–3467. DOI: 10.1103/physreva.52.3457.

[21] G. Dresselhaus. “Spin-Orbit Coupling Effects in Zinc Blende Structures”. In: *Phys. Rev.* 100.2 (1955), pp. 580–586. DOI: 10.1103/physrev.100.580.

[22] Y. A. Bychkov and E. I. Rashba. In: *JETP. Lett.* 39.78 (1984).

[23] D. M. Zumbühl et al. “Spin-Orbit Coupling, Antilocalization, and Parallel Magnetic Fields in Quantum Dots”. In: *Phys. Rev. Lett.* 89.27 (2002), p. 276803. DOI: 10.1103/physrevlett.89.276803.

[24] S. Amasha et al. “Electrical Control of Spin Relaxation in a Quantum Dot”. In: *Phys. Rev. Lett.* 100.4 (2008), p. 046803. DOI: 10.1103/physrevlett.100.046803.

[25] Vitaly N. Golovach, Alexander Khaetskii, and Daniel Loss. “Phonon-Induced Decay of the Electron Spin in Quantum Dots”. In: *Phys. Rev. Lett.* 93.1 (2004), p. 016601. DOI: 10.1103/physrevlett.93.016601.

[26] R. Hanson et al. “Spins in few-electron quantum dots”. In: *Rev. Mod. Phys.* 79.4 (2007), pp. 1217–1265. DOI: 10.1103/revmodphys.79.1217.

[27] D. Paget et al. “Low field electron-nuclear spin coupling in gallium arsenide under optical pumping conditions”. In: *Phys. Rev. B* 15.12 (1977), pp. 5780–5796. DOI: 10.1103/physrevb.15.5780.

[28] Alexander V. Khaetskii, Daniel Loss, and Leonid Glazman. “Electron Spin Decoherence in Quantum Dots due to Interaction with Nuclei”. In: *Phys. Rev. Lett.* 88.18 (2002), p. 186802. DOI: 10.1103/physrevlett.88.186802.

[29] I. A. Merkulov, Al. L. Efros, and M. Rosen. “Electron spin relaxation by nuclei in semiconductor quantum dots”. In: *Phys. Rev. B* 65.20 (2002), p. 205309. DOI: 10.1103/physrevb.65.205309.

[30] R. Ziegler, C. Bruder, and Herbert Schoeller. “Transport through double quantum dots”. In: *Phys. Rev. B* 62.3 (2000), pp. 1961–1970. DOI: 10.1103/physrevb.62.1961.

[31] J. R. Petta. “Coherent Manipulation of Coupled Electron Spins in Semiconductor Quantum Dots”. In: *Science* 309.5744 (2005), pp. 2180–2184. DOI: 10.1126/science.1116955.

[32] Marek Korkusinski et al. “Topological Hunds rules and the electronic properties of a triple lateral quantum dot molecule”. In: *Phys. Rev. B* 75.11 (2007), p. 115301. DOI: 10.1103/physrevb.75.115301.

[33] J. M. Taylor, V. Srinivasa, and J. Medford. “Electrically Protected Resonant Exchange Qubits in Triple Quantum Dots”. In: *Phys. Rev. Lett.* 111.5 (2013), p. 050502. DOI: 10.1103/physrevlett.111.050502.

[34] J. Medford et al. “Quantum-Dot-Based Resonant Exchange Qubit”. In: *Phys. Rev. Lett.* 111.5 (2013), p. 050501. DOI: 10.1103/physrevlett.111.050501.

[35] R. Maurand et al. “A CMOS silicon spin qubit”. In: *Nat. Commun.* 7.1 (2016). DOI: 10.1038/ncomms13575.

[36] Arnau Sala and Jeroen Danon. “Leakage and dephasing in Si28 -based exchange-only spin qubits”. In: *Phys. Rev. B* 98.24 (2018), p. 245409. DOI: 10.1103/physrevb.98.245409.

[37] Arnau Sala and Jeroen Danon. “Exchange-only singlet-only spin qubit”. In: *Phys. Rev. B* 95.24 (2017), p. 241303. DOI: 10.1103/physrevb.95.241303.

[38] C. Zener. “Non-Adiabatic Crossing of Energy Levels”. In: *Proceedings of the Royal Society A: Mathematical, Physical and Engineering Sciences* 137.833 (1932), pp. 696–702. DOI: 10.1098/rspa.1932.0165.

[39] John Schliemann, Alexander Khaetskii, and Daniel Loss. “Electron spin dynamics in quantum dots and related nanostructures due to hyperfine interaction with nuclei”. In: *J. Phys. Condens. Matter* 15.50 (2003), R1809–R1833. DOI: 10.1088/0953-8984/15/50/r01.

[40] M. Kotur et al. “Spin-lattice relaxation of optically polarized nuclei in p -type GaAs”. In: *Phys. Rev. B* 97.16 (2018), p. 165206. DOI: 10.1103/physrevb.97.165206.

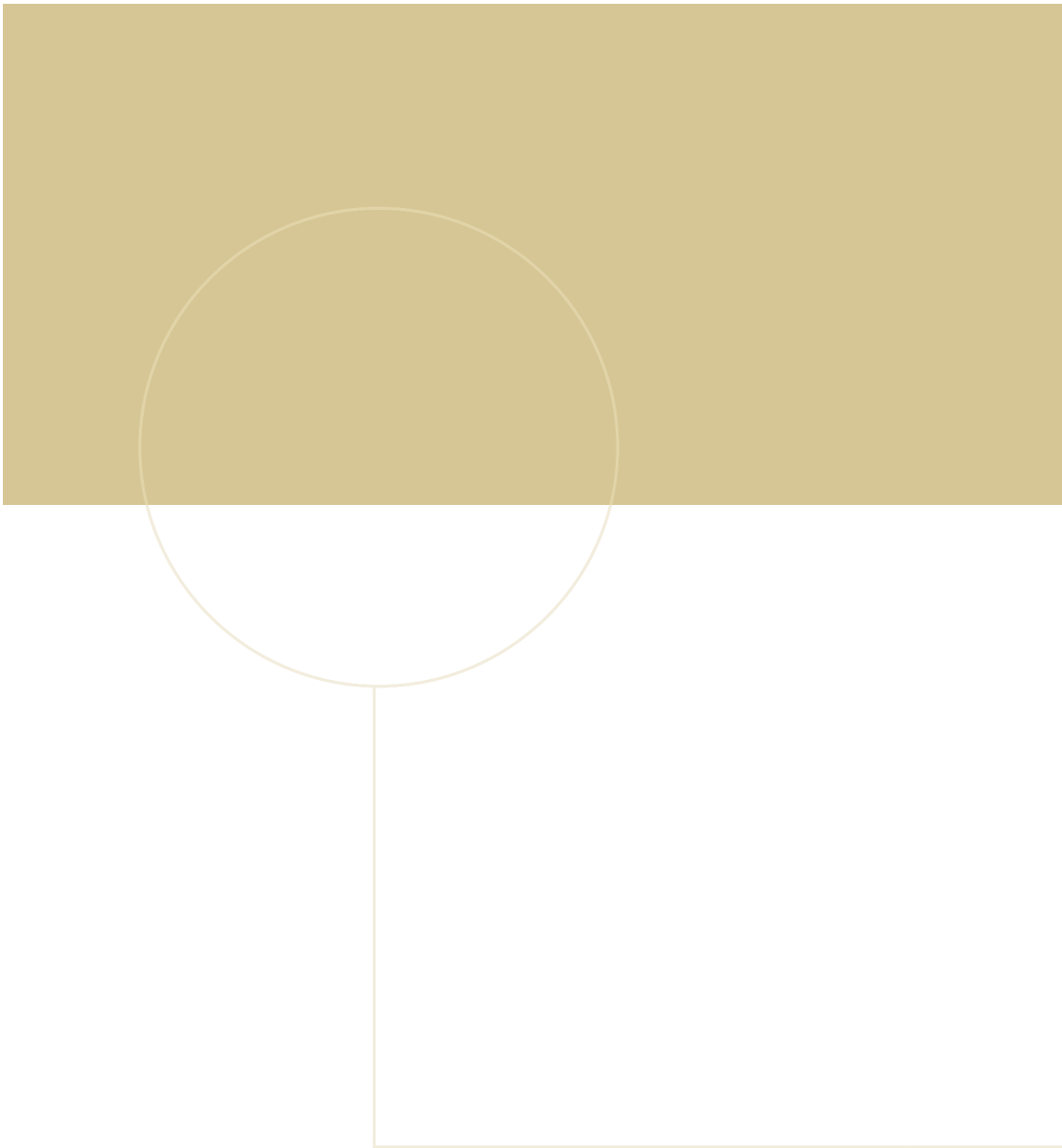

NTNU

Kunnskap for en bedre verden